Annu. Rev. Phys. Chem. 2001. 52:315–56

FAST PROTEIN DYNAMICS PROBED WITH INFRARED VIBRATIONAL ECHO EXPERIMENTS

Michael D Fayer
Department of Chemistry, Stanford University, Stanford, California 94305; e-mail: fayer@fayerlab.stanford.edu

Key Words pure dephasing, protein glass transition, protein viscosity dependence, protein surface fluctuations

■ **Abstract** IR vibrational echo experiments are used to study dynamics in myoglobin (Mb) by investigating the dephasing of the CO-stretching mode of CO bound at the active site of the protein (Mb-CO). The temperature dependence and the viscosity dependence of Mb-CO pure dephasing have been measured in several solvents. In low-temperature, glassy solvents, the pure dephasing has a power law temperature dependence, $T^{1.3}$, that reflects glasslike protein dynamics. In liquids, the temperature dependence is much steeper and arises from a combination of pure temperature dependence and the influence of decreasing solvent viscosity with increasing temperature. As the solvent viscosity decreases, the ability of the protein's surface to undergo topological fluctuations increases, which in turn increases the internal protein-structural fluctuations. The protein-structural motions are coupled to the CO bound at the active site by electric field fluctuations that accompany movements of polar residues. The dynamic electric field-coupling mechanism is tested by observing differences in the temperature dependence of the pure dephasing of Mb-CO mutations.

INTRODUCTION

In 1993, the first ultrafast vibrational echo experiments were performed on condensed-matter systems, using tunable IR pulses (1). The development and application of ultrafast IR vibrational echoes and other IR coherent-pulse sequences are providing a new approach to the study of the structural states of molecules in complex molecular systems such as liquids, glasses, and proteins (2–11). The vibrational echo experiments and related ultrafast vibrational-coherence experiments are outgrowths of advances made in magnetic resonance methods and coherent optical spectroscopy over many decades.

NMR spin echo experiments, first performed in 1950, began a new era in spectroscopy (12). The spin echo was the first spectroscopic experiment to take advantage of coherent interactions of a radiation field with the system to obtain information not available in an absorption measurement. The spin echo is the

simplest of all pulsed magnetic resonance experiments. It involves the application of two radio frequency pulses and observation of the time-dependent response of the sample. Since 1950, a large number of complex pulse sequences have been developed and applied to the study of magnetic spin systems (13). All of these have direct lineage to the earlier spin echo experiments.

In 1964, photon echo experiments extended spin echo experiments to electronically excited states (14, 15). The photon echo began the application of coherent-pulse techniques in the visible and UV portions of the electromagnetic spectrum. Since its development, the photon echo and related pulse sequences have been applied to a wide variety of problems including dynamics and intermolecular interactions in crystals, glasses, proteins, and liquids (16–19). Like the spin echo, the photon echo and other optical, coherent-pulse sequences provide information that is not available from absorption or fluorescence spectroscopy.

The spin echo, the photon echo, and the vibrational echo are, in many respects, similar experiments. The term vibrational echo is used to distinguish IR experiments on vibrations from radio frequency experiments on spins or visible and UV experiments on electronic states. In this chapter, recent vibrational echo experiments on the proteins myoglobin (Mb) and hemoglobin (Hb) are described.

The dynamics of proteins on a wide variety of time scales are intimately related to protein function. Fast and moderately fast fluctuations of protein structure enable a protein to sample a complex conformational-energy landscape. These rapid motions give rise to the slower processes associated with protein function. Molecular-dynamics simulations have shown that a protein can sample thousands of conformations within a very short time (20, 21). Understanding these dynamics provides an important connection between protein function and protein structure, as determined by X ray (22, 23), NMR (24, 25), and other experimental techniques (26–30) and theory (20, 21).

The importance of dynamic fluctuations in proteins is illustrated by Mb, which is a 153-amino-acid protein with the primary biological function of reversibly binding and transporting O_2 in muscle tissue. The ability of Mb to bind O_2 and other biologically relevant ligands, such as CO or NO, results from a nonpeptide prosthetic group, heme, which is located in the protein's "pocket" and is covalently bound at the proximal histidine (H93) of the globin protein. The X-ray crystal structure of Mb indicates that there are no static gaps for ligands to pass through (31). For ligands to move in and out of the pocket, they must traverse the intervening protein. Traversing the protein is made possible at room temperature by dynamic fluctuations in the protein structure that open paths for ligand diffusion through the protein (32). Because of the ability of ligands to move through the protein, in some sense, the protein has liquidlike character at room temperature (32).

Vibrational echo experiments can be applied to Mb by examining the dynamics of the CO ligand bound at the active site of the protein (Mb-CO). The vibrational levels of a molecular oscillator in a condensed-matter system are influenced by the surrounding medium through intermolecular interactions. The time-averaged forces exerted by the solvent on an oscillator cause a static shift in the

vibrational-absorption frequency relative to its frequency in the gas phase. The frequency shifts of the vibrational transitions of a molecule between the gas phase and a condensed-matter environment are indicators of the effect of the solvent on the internal mechanical degrees of freedom of a solute.

The fluctuating forces exerted by a medium also produce fluctuations in the molecular structure. Such structural fluctuations cause the vibrational eigenstates to be time dependent, and, thus, the vibrational-energy eigenvalues are time dependent. Time evolution of the vibrational-energy eigenvalues produces fluctuations in the vibrational-transition energies. Structural fluctuations and the associated energy fluctuations are not generally observable in either an IR or Raman vibrational spectrum. The extent and time dependence of the fluctuations of a molecular oscillator's vibrational-energy levels are sensitive to the nature of the dynamics of the condensed-matter environment and the strength of intermolecular interactions. In Mb-CO, protein-structural fluctuations are responsible for the time dependence of the CO energy levels.

In principle, information on dynamical intermolecular interactions of an oscillator with its environment can be obtained from vibrational-absorption spectra. The forces experienced by the oscillator determine the vibrational line shape and width. The IR absorption line shape is related to these microscopic dynamics through the Fourier transform of the two-time transition dipole correlation function (33–36), which includes any inhomogeneous broadening (33, 34, 36). The line shape and width depend on temperature and other properties of the environment that influence the oscillator. However, a vibrational-absorption spectrum reflects the full range of mechanisms that broaden the vibrational line shape, including dynamical contributions and static or essentially static inhomogeneous contributions to the line shape (33–36). In proteins such as Mb-CO and Hb-CO, inhomogeneous broadening of the CO vibrational transition exceeds the dynamical line width (10, 37). Under these circumstances, measurements of absorption spectra do not provide information on protein dynamics.

The vibrational echo experiment is a coherent IR pulse sequence that removes inhomogeneous broadening from the vibrational transition and reveals the underlying dynamical line shape. In contrast to an IR absorption spectrum, the vibrational echo is described by a four-time correlation function (18, 38, 39). The vibrational echo is one of a class of spectral line-narrowing experiments described by a four-time correlation function (18).

In a vibrational echo experiment, a source of short IR pulses is tuned to the vibrational transition of interest. The vibrational echo employs a two-pulse excitation sequence. The first pulse places each solute molecule's vibration into a superposition state, which is a mixture of the $\nu = 0$ and $\nu = 1$ vibrational levels. Each vibrational superposition has a microscopic electric dipole associated with it. This dipole oscillates at the vibrational-transition frequency. Immediately after the first pulse, all of the microscopic dipoles in the sample oscillate in phase. Because there is an inhomogeneous distribution of vibrational-transition frequencies, the individual dipoles oscillate with some distribution of frequencies. Thus,

the initial-phase relationship is very rapidly lost. This is referred to as the free-induction decay. After a time τ, a second pulse, traveling along a path that makes an angle θ with that of the first pulse, passes through the sample. This second pulse changes the phase factors of each vibrational-superposition state in a manner that initiates a rephasing process. At time τ after the second pulse, the sample emits a third coherent pulse of light. The emitted pulse propagates along a path that makes an angle of 2θ with the path of the first pulse. The third pulse is the vibrational echo. It is generated when the ensemble of microscopic dipoles (one for each vibrational oscillator) is rephased at time 2τ. The phased array of microscopic dipoles behaves as a macroscopic oscillating dipole, which generates an IR pulse of light. A free-induction decay (inhomogeneous frequency distribution) again destroys the phase relationships, so only a short pulse of light is generated.

The rephasing at 2τ has removed the effects of the inhomogeneous broadening. However, fluctuations due to coupling of the vibrational mode (CO vibration) to the heat bath (protein-structural dynamics) cause the oscillation frequencies also to fluctuate. Thus, at 2τ there is not perfect rephasing. As τ is increased, the fluctuations produce increasingly large accumulated phase errors among the microscopic dipoles, and the size of the vibrational echo is reduced. A measurement of the vibrational echo intensity vs τ, the delay time between the pulses, is called a vibrational echo decay curve. Thus, the vibrational echo decay is related to the fluctuations in the vibrational frequencies, not the inhomogeneous spread in frequencies. The Fourier transform of the vibrational echo decay yields the underlying dynamical line shape (40, 41). For example, if the vibrational echo decay is exponential, the line shape is Lorentzian, and the line width is determined by the exponential decay constant. The vibrational echo makes the vibrational-dynamic line shape experimentally observable. In fact, the vibrational echo decay measures directly the decay of the system's off-diagonal density matrix elements and is the fundamental observable.

To obtain a physical feel for the manner in which the vibrational echo experiment can reveal homogeneous fluctuations despite a broad inhomogeneous spread of transition frequencies, consider the following foot race scenario (42, 43). Initially, all of the runners in this scenario are lined up at the starting line (see Figure 1). At $t = 0$, the starting gun (analogous to the first IR pulse) is fired, and the runners take off down the track. After running for some time, the faster runners are out in front, and the slower runners are somewhat behind. The runners are no longer in a line because of the inhomogeneity of their speeds. At time τ, the gun is again fired (analogous to the second IR pulse), and all of the runners turn around and run back toward the starting line. If each runner maintains a constant speed out and back, then all of the runners will cross the starting line exactly in line again (see Figure 1, second panel from bottom). When the second gun is fired, the faster runners are farther away from the starting line than the slower runners, but because fast runners run more quickly, the differences in distances are exactly made up for by the differences in speeds. At the starting line, the group is "rephased"; the inhomogeneity in speeds is nullified. If the runners do not run at exactly constant

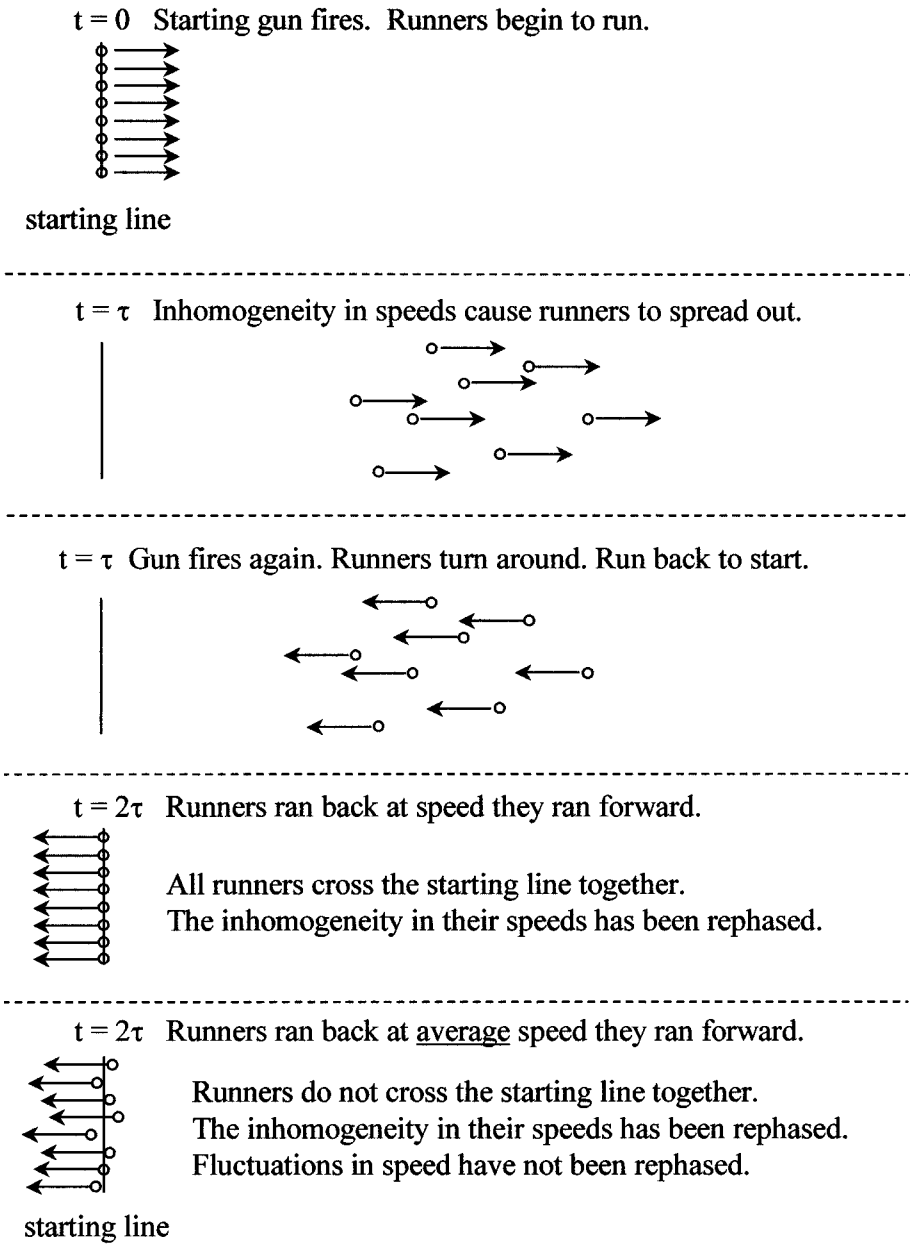

Figure 1 Analogous use of runners on a racetrack to illustrate the mechanism by which a vibrational echo experiment eliminates inhomogeneous broadening and permits measurement of pure dephasing (energy level fluctuations). The first and second firings of the starting gun correspond to the first and second pulses in the vibrational echo pulse sequence. See text for other details.

speeds, but each runner has some fluctuation in speed about his average (dynamical fluctuations), then the runners will not cross the starting line exactly in a line (see Figure 1, bottom panel). The rephasing will be imperfect. A snapshot of the group as it crosses the starting line on the return leg of the race will show a spread in positions about the starting line, revealing the small fluctuations in the runners' speeds. If the runners run out for a longer time (τ is increased), then the fluctuations will produce a greater spread in positions about the starting line. The increase in the spread as τ is increased is a measure of the fluctuations in the speeds, and the measurement is not influenced by the inhomogeneity in the speeds. In the same manner, the vibrational echo experiment reveals the fluctuations in the vibrational-transition frequency despite a large inhomogeneous distribution of vibrational energies.

Recently, the ultrafast IR vibrational echo technique has been applied to the study of Mb-CO dynamics (4, 5, 7, 10, 44) and those of the closely related protein Hb-CO (37). The vibrational echo measurements of the pure dephasing of the CO-stretching mode are sensitive to the complex protein dynamics communicated to the CO ligand bound at the active site of the protein. Unlike other ultrafast techniques (45, 46), which involve electronic excitation of chromophores, the vibrational echo experiments directly examine effects of fluctuations of protein structure on the ground state potential-energy surface.

In this review, first some details of the vibrational echo experiments and experimental procedures are presented. Then some of the basic data taken on Mb-CO are discussed, and a model is presented for the mechanism that couples protein fluctuations to CO bound at the active site and causes CO vibrational dephasing. Experiments on mutant Mbs are used to support the model (5, 7). Then data on the temperature dependence of the dephasing of Mb-CO are presented. At low temperatures in glassy solvents, the temperature dependence is a power law, $T^{1.3}$. This temperature dependence is suggestive of glasslike dynamics, and there is evidence of a protein "glass transition" at $\sim$200 K (10). The solvent viscosity dependence of the Mb-CO dephasing is analyzed. A viscoelastic model is used to describe the data (47). The results demonstrate the importance of fluctuations of the protein's surface in determining the extent of internal-protein dynamics. Finally, results of experiments on Hb-CO are compared with the results on Mb-CO.

THE VIBRATIONAL ECHO METHOD AND EXPERIMENTAL PROCEDURES

The Vibrational Echo Method

The Mb-CO absorption spectrum (1945 cm^{-1}) is inhomogeneously broadened, even at room temperature. The line shape reflects the distribution of quasistatic protein configurations that give rise to a range of CO frequencies, but the line shape provides no information about the protein dynamics. The vibrational echo is a two-pulse time domain technique that is sensitive to the dynamics of the CO frequency and thus can provide information on the protein dynamics.

Standard treatments of echo spectroscopy (or line shapes) describe two extreme limits (40, 48, 49)—very fast processes, which produce homogeneous dephasing and a motionally narrowed spectroscopic line, and very slow or static processes, which produce an inhomogeneously broadened spectroscopic line. In standard applications, the echo experiment extracts the homogeneous line width (dephasing rate) from a transition dominated by inhomogeneous broadening. In this case, the echo decay is given by

$$S_E(\tau) = S_E(0)e^{-4\tau/T_E}, \qquad 1.$$

and the experimental echo decay time T_{E} is equal to the ensemble averaged homogeneous dephasing time T_2 in the sense of the Bloch equations. The homogeneous line width is $(\pi T_2)^{-1}$ (40).

A common source of homogeneous dephasing is continuous frequency modulations that produce motional narrowing. For processes that cause motional narrowing, the modulation time τ_{m} of the fast process is fast compared with the typical size of the frequency perturbation Δ_{m} (the rms range of frequencies sampled); that is, $\Delta_{\mathrm{m}}\tau_{\mathrm{m}} \ll 1$ (50, 51). Under these conditions, the echo measures the dephasing time ${T_{\mathrm{E}}}^{-1} = {T_2}^{-1} = {\Delta_{\mathrm{m}}}^2\tau_{\mathrm{m}}$ (49). It does not measure the modulation time directly, although T_{E} and τ_{m} can be related by an appropriate model.

At the other limit, the slow process is assumed to be essentially static. It has no effect on the echo decay, but it does contribute to the absorption line width. If the typical size of the quasistatic frequency variation is Δ_{I}, the Fourier transform of the absorption line shape, often called a free-induction decay, is

$$S_{FID}(\tau) = S_{FID}(0)e^{-\Delta_I^2\tau^2/2}e^{-4\tau/T_2}. \qquad 2.$$

If the inhomogeneous line width Δ_{I} is large, no information on the dephasing time or the modulation times of the system can be obtained from the line shape. However, the echo can extract the value of T_2, which is related to the system's dynamics.

The effect of the vibrational population lifetime T_1 is removed by combining the vibrational echo time T_{E} with a pump probe measurement (transient absorption) of T_1 to yield the pure dephasing time T_E^* through

$$\frac{1}{T_E} = \frac{1}{T_E^*} + \frac{1}{2T_1}. \qquad 3.$$

The pure dephasing time T_E^* is caused only by CO transition frequency fluctuations, which in turn are caused by the protein dynamics.

A variety of physical processes conform to this standard model, that is, there is a vast separation of time scales that produces a homogeneous line (not necessarily motionally narrowed) that underlies an inhomogeneously broadened absorption spectrum. Examples include absorption spectra and photon echo experiments on chromophores in low-temperature glasses (19), in which the pure dephasing is caused by two-level system (TLS) dynamics (52, 53) and possibly IR absorption

spectra and vibrational echo experiments on proteins at moderate to low temperatures (10). The low-temperature and viscosity-independent processes seen in the experiments below fit this model. However as discussed below, the viscosity-dependent portion of the dephasing does not fit the model (54).

The standard model is adequate if the dynamics are either very fast or very slow. However, there is also a broad range of modulation times between these limits, in which the vibrational echo behaves quite differently from these standard treatments. In this intermediate range, the modulation time is long enough to prevent motional narrowing ($\Delta_m \tau_m \gg 1$), but it is not slow enough for its effects to be eliminated from the two-pulse echo experiment; that is, Δ_m is not part of the inhomogeneous line. A process that occurs in this intermediate time range produces what is called spectral diffusion, that is, relatively slow evolution of the vibrational frequency. Spectral diffusion can be studied using three-pulse stimulated echoes (40, 48, 49, 55) or the time-dependent versions of hole burning or fluorescence line narrowing (18, 19, 56). However, with proper interpretation, the two-pulse echo also becomes a powerful tool for measuring spectral diffusion (47, 54).

Relatively little attention has been paid to two-pulse echoes in the spectral-diffusion range. Older work focused on models appropriate for spin resonance (57–59). After the basic results of Yan & Mukamel (60), a more detailed examination of the behavior of the two-pulse echo as the modulation time is varied has been presented (54). When τ_m is in the spectral-diffusion range, the echo decay time T_E is no longer equal to a dephasing time T_2 in the sense of the Bloch equations, and the echo decay time is related to an inverse dynamic line width that is not the equivalent of the standard homogeneous line width. In the spectral-diffusion regimen, the echo decay is more directly related to the underlying modulation time τ_m. In general, if the initial decay of the frequency-frequency correlation function has the form $1 - {\tau_m}^{\beta}$ (the short time expansion of a variety of time-dependent functions, for example, an exponential, a Gaussian, and a stretched exponential), then (54)

$$\Delta_m T_E = B_\beta \Gamma\left(\frac{1}{\beta+2}\right)(\Delta_m \tau_m)^{\beta/(\beta+2)}, \qquad 4.$$

and

$$B_\beta = \frac{1}{2}\left(\frac{8}{\beta+2}\right)^{\frac{\beta+1}{\beta+2}}\left(\frac{\beta+1}{2^\beta-1}\right)^{\frac{1}{\beta+2}}. \qquad 5.$$

In the specific case of an exponentially decaying frequency-frequency correlation function, $\beta = 1$, and Yan & Mukamel's result is recovered (60):

$$T_E = \left(\frac{4}{3}\right)^{2/3}\Gamma(1/3)\left(\frac{\tau_m}{\Delta_m^2}\right)^{1/3}. \qquad 6.$$

In these equations, the standard gamma function Γ is used, and T_E is defined as the integral decay time (54). The weak cube-root dependence, $T_E \propto \tau_m^{1/3}$, makes the echo useful over a very wide range of modulation times. It is also very different from the $T_E \propto \tau_m^{-1}$ dependence expected in the motionally narrowed limit. The

data presented below on the viscosity-dependent pure dephasing of Mb-CO follow $T_E \propto \tau_m^{1/3}$, implying that the protein-structural fluctuations occur on intermediate time scales and cause viscosity-dependent spectral diffusion of the CO vibrational frequency.

Experimental Procedures

The IR vibrational echo experiments on Mb-CO (most of the experiments) were performed by using the Stanford free-electron laser (FEL). The FEL produces tunable, ps-duration, mid-IR pulses. The experiments on Hb-CO were performed using a Ti:Sapphire-based optical-parametric-amplifier (OPA) system to generate tunable sub-ps-duration mid-IR pulses (37). The IR pulses from the FEL had energies of $\sim$0.5 μJ and were nearly transform-limited Gaussian distributions of 1.2 ps in duration. Both the autocorrelation and the spectrum of the IR pulse were monitored continuously during the experiments. The spot size in the sample was $\sim$100 μm. The energies at the sample in the two pulses of the echo sequence were $\sim$50 and $\sim$150 nJ, respectively. The vibrational lifetime T_1 was measured by pump probe experiments (transient absorption).

The FEL experimental apparatus is shown in Figure 2 (61, 62). The IR beam enters the experimental area roughly collimated. L1 and L2 reduce the beam size. At the focus of the telescope is a Ge acousto-optic modulator (AOM) for pulse selection, within a 1:1 cylindrical telescope using CaF_2 lenses. Micropulses are selected out of each FEL macropulse ($\sim$2 ms in duration at a 10 Hz repetition rate

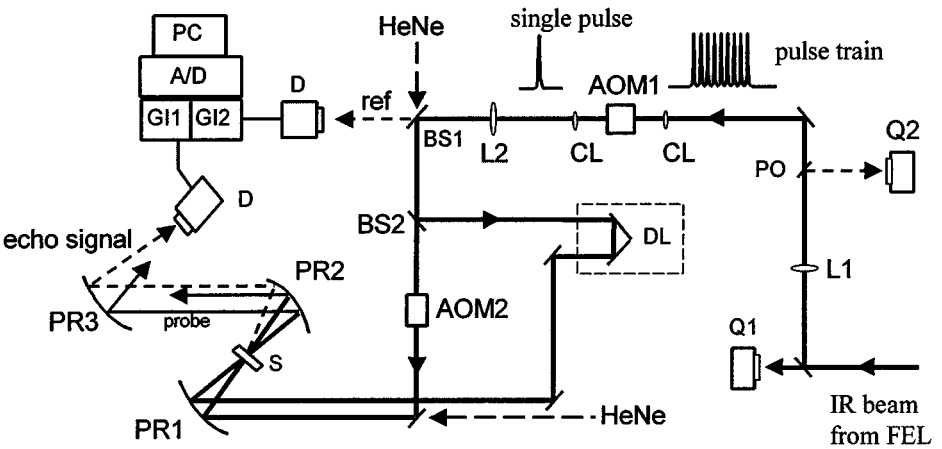

Figure 2 Vibrational echo experimental setup when using the Stanford free-electron laser (*FEL*) as the source of IR pulses. Pulse selection is accomplished with an acousto-optic modulator 1 (*AOM1*), while *AOM2* is used for chopping of pulse 2. *A/D*, analog-to-digital converter; *BS*, ZnSe beam splitter; *CL*, cylindrical lens; *D*, detector; *DL*, optical delay line; *GI*, gated integrator; *L*, lens; *PC*, computer; *PO*, pick-off; *PR*, off-axis parabolic reflector; *Q*, position-sensitive detector; *S*, sample.

with micropulses occurring at 12 MHz) at a repetition rate of 50 kHz by the AOM single-pulse selector. The cylindrical telescope makes the AOM rise time less than the interpulse separation. The pulse selection yields an effective experimental repetition rate of 1 kHz, and an average power of <0.5 mW. A ZnSe beam splitter allows 1% of the IR beam to be directed into an HgCdTe reference detector. All data from pulses with intensities outside a 10% window were discarded.

The two pulses for vibrational echo or pump probe experiments were obtained with a 10% ZnSe beam splitter. The 10% beam (first pulse in the vibrational echo sequence and probe pulse) is sent through a computer-controlled stepper motor delay line. The remaining portion (second vibrational echo pulse or pump pulse) is chopped at 25 kHz with a second Ge AOM. A HeNe beam is made collinear with each IR beam for alignment purposes. The two pulses were focused using an off-axis parabolic reflector, for achromatic focusing of the IR and HeNe. The beams and vibrational echo signal were recollimated with a second parabolic reflector and focused into a HgCdTe signal detector with a third parabolic reflector. By selecting the desired beam with an iris between the second and third parabolic reflectors, either the vibrational echo or pump probe signal could be observed. The vibrational echo signal and the intensity reference signal were sampled by two gated integrators and digitized for collection by computer. Careful studies of power dependence and repetition rate dependence of the data were performed. It was determined that there were no heating or other unwanted effects.

The measurements were made on native horse heart Mb (Sigma; used without further purification). Samples were prepared by adding 15 mM lyophilized Mb-Fe^{+3} to either 50:50, 80:20, or 95:5 wt% glycerol–0.1 M phosphate buffer (pH 7) or 50:50 (vol/vol) ethylene glycol–0.1 M phosphate buffer (pH 7). The resulting solutions were then stirred under CO atmosphere for 8 h before being reduced by a 10-fold molar excess of dithionite.

The water sample was prepared in the same manner except that the concentration was 30 mM in 0.1 M phosphate buffer (pH 7). The trehalose sample was prepared by making an $\sim$10 wt% solution of trehalose in 0.1 M phosphate buffer (pH 7) and dissolving Mb-Fe^{+3} in it to a final concentration of 1–2 mM. A few drops of the resulting solution were placed on a sapphire window and allowed to dry under CO atmosphere for a few days. Another sapphire window was pushed against the first one to give a thickness of $\sim$100 μm.

The viscosity measurements were performed with Cannon-Ubbelohde viscometers. For the Mb-CO in 50:50 ethylene glycol-water, temperature-dependent-viscosity measurements were made in a variety of low temperature baths (47). To obtain the viscosity, η, at lower temperatures, a Vogel-Tammann-Fulcher (VTF) equation (63–65) was used to model the viscosity at all temperatures. A fit was made to the measured points to yield (47)

$$\eta = (2.0 \times 10^{-4}\ \text{cP}) \exp\left(-\frac{2500\ \text{K}}{T - 70\ K}\right). \qquad 7.$$

However, a single VTF curve cannot accurately emulate the viscosity over such a

large temperature range. Therefore, the viscosities at the lowest temperatures are approximate.

RESULTS AND DISCUSSION

The Data on Mb-CO

Figure 3*a* shows a vibrational echo decay of Mb-CO in the solvent trehalose glass at 11 K (10). The signal-to-noise ratio is excellent despite a large background absorption by the protein and the trehalose. The Mb-CO peak has an optical density ~0.2 on a background of optical density 1. The data are fit well by a 7.0-ps decay constant exponential curve, which corresponds to a homogeneous dephasing time of 28 ps and a homogeneous width of 0.38 cm^{-1}. At room temperature, the dynamical width increases to ~2 cm^{-1}. The full absorption line width at half maximum is ~15 cm^{-1} at all temperatures. Therefore, the Mb-CO absorption line is inhomogeneously broadened at all temperatures studied, and dynamical information could not be obtained from an absorption spectrum.

Figure 3*b* is a semilog plot of the temperature dependence in trehalose of T_E (*circles*), $2T_1$ (*squares*), and T_E^* (*triangles*). T_E^* was computed from the other two quantities, using Equation 3. T_1 has a slight, essentially linear temperature dependence. It can be seen that, at low temperatures, the vibrational echo decay is nearly lifetime limited. By room temperature, the vibrational echo decay is dominated by pure dephasing.

Figure 4 displays temperature-dependent pure dephasing line widths, $1/\pi T_E^*$, for Mb-CO in glycerol/water. At low temperature, the data were a power law with temperature dependence $T^{1.3}$. The power law is shown more clearly below. At higher temperature, the functional form of the data changes; the temperature dependence becomes steeper. A detailed discussion of the temperature and solvent viscosity dependence is given below. First, the mechanism that couples time dependent structural fluctuations of the protein to the CO vibrational frequency to produce pure dephasing is described.

Protein Structural Dynamics and CO Dephasing: Mutant Studies

In the various experiments, Mb-CO is dissolved in a variety of liquid and glassy solvents. The solvent viscosity plays an important role in determining the nature and extent of the Mb structural fluctuations that contribute to pure dephasing. However, the solvent does not directly couple to the CO, which is bound at the active site. The Mb pocket protects the CO from direct interaction with the solvent.

For the solvent to cause dephasing, its motions must couple to the transition frequency of the CO. When molecules go from the gas phase to a condensed phase, there is a shift of electronic and vibrational-transition frequencies. This effect is referred to as the solvent shift. Intermolecular interactions with the

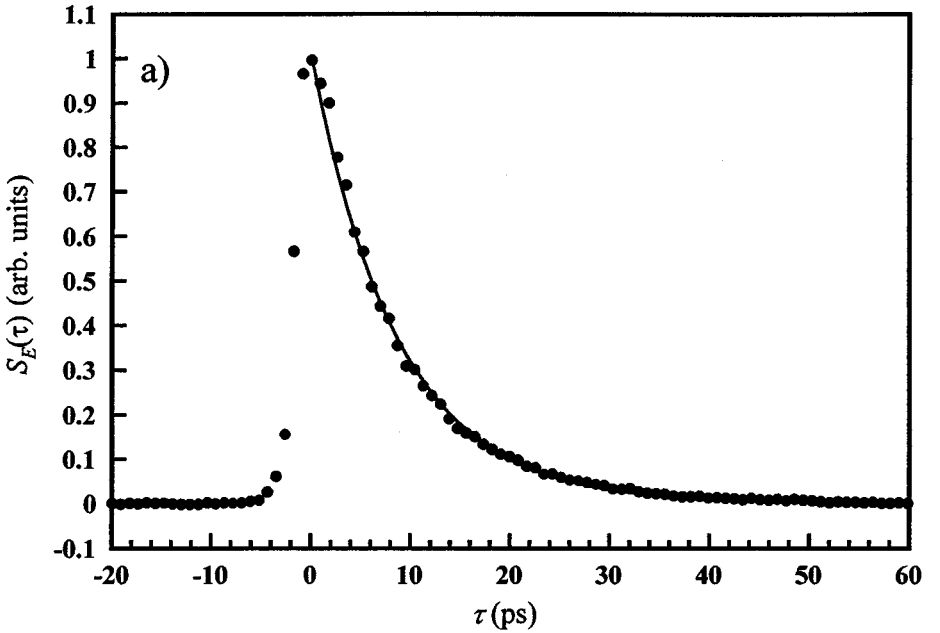
a)
$S_E(\tau)$ (arb. units)
τ (ps)
1.1
1
0.9
0.8
0.7
0.6
0.5
0.4
0.3
0.2
0.1
0
-0.1
-20
-10
0
10
20
30
40
50
60

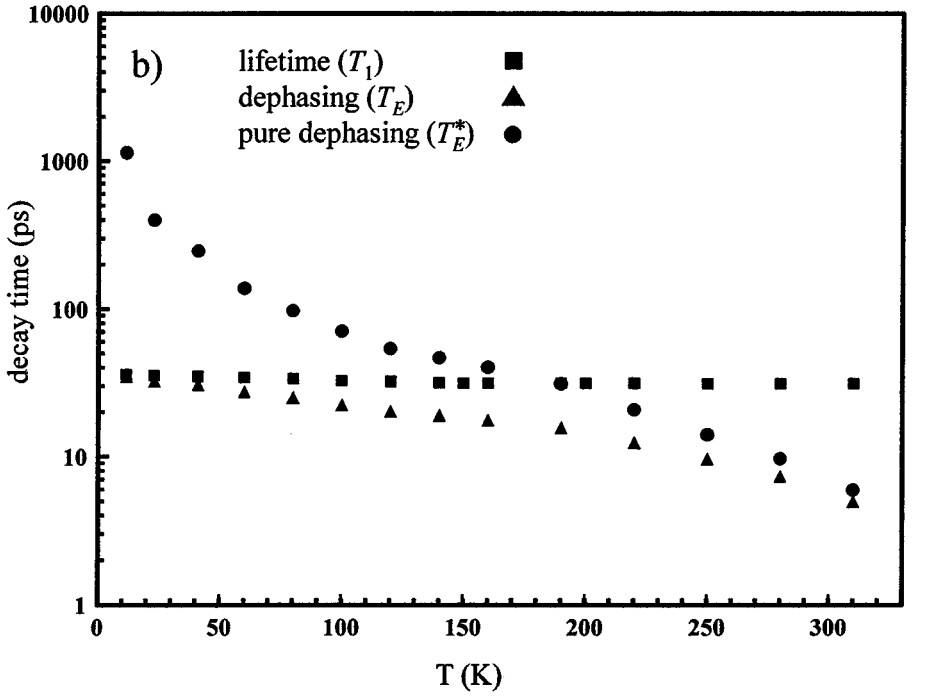
b)
lifetime (T_1)
dephasing (T_E)
pure dephasing (T_E^*)
decay time (ps)
T (K)
10000
1000
100
10
1
0
50
100
150
200
250
300

condensed-matter environment are responsible for line broadening as well as the solvent shift. These phenomena are closely related. The line broadening can be static, giving rise to an inhomogeneous line, or dynamic. In either case, it is the variations in the solvent shift that cause line broadening.

In Mb-CO, the nature of the solvent itself has little effect on the CO vibrational-transition frequency. The Mb-CO transition frequency is virtually identical in a wide variety of liquids and glasses (66, 67). The solvent shift is unaffected by the medium surrounding the protein, even when the change is from a liquid solvent such as water or a mixture of glycerol and water to a protein crystal (67). In contrast, the frequency difference between the A_0 and A_1 CO absorption lines in Mb-CO is 24 cm^{-1} (66). This difference in the CO absorption frequency is caused by a change in conformation of the protein, particularly the position of the distal histidine, an amino acid close to the CO. Changes in the protein structure can have a major influence on the CO vibrational frequency, whereas changes in the solvent have a negligible influence. This spectroscopic information leads to the reasonable conclusion that fluctuations of the protein structure will cause pure dephasing, while fluctuations of the solvent structure will not. The solvent does provide a heat bath and a boundary condition that are intimately involved in the protein fluctuations and the dephasing, but the argument made above strongly supports the idea that the dephasing does not arise from direct coupling of the solvent dynamics to the CO transition frequency.

The $T^{1.3}$ power law pure-dephasing temperature dependence displayed in Figure 4 is also observed in several other solvents (10; see below). The power laws in the various solvents have the same slopes and the same values of the pure dephasing rates, showing that the dephasing is not affected by the specific chemical composition of the solvent. This fact is another demonstration that the solvent does not directly interact with the CO to produce pure dephasing. Rather, the vibrational dephasing is caused by protein-structural fluctuations (5, 7, 62).

The manner in which the Mb protein fluctuations are communicated to the CO bound at the active site and in which they produce pure dephasing has been described previously (5, 7, 47, 62). A model was developed that ascribes the CO vibrational pure dephasing to global structural fluctuations of the protein. The protein-structural dynamics produce fluctuating electric fields because polar groups throughout the protein are moving. The fluctuating electric fields cause the CO vibrational frequency to fluctuate via the Stark effect (68). A number of detailed quantum chemical studies (69, 70) and experimental studies (68) demonstrate that changes in the electric field act directly on the CO, changing its frequency through the Stark effect. The theoretical and experimental studies are for static changes in

Figure 3 (*a*) Vibrational echo decay data for Mb-CO in trehalose. The line through the data is a fit to a single exponential. (*b*) Mb-CO lifetime data ($2T_1$), vibrational echo data (T_E), and pure dephasing data (T_E^*) as a function of temperature. The pure-dephasing data are obtained by removing the T_1 contribution from T_E, using Equation 3.

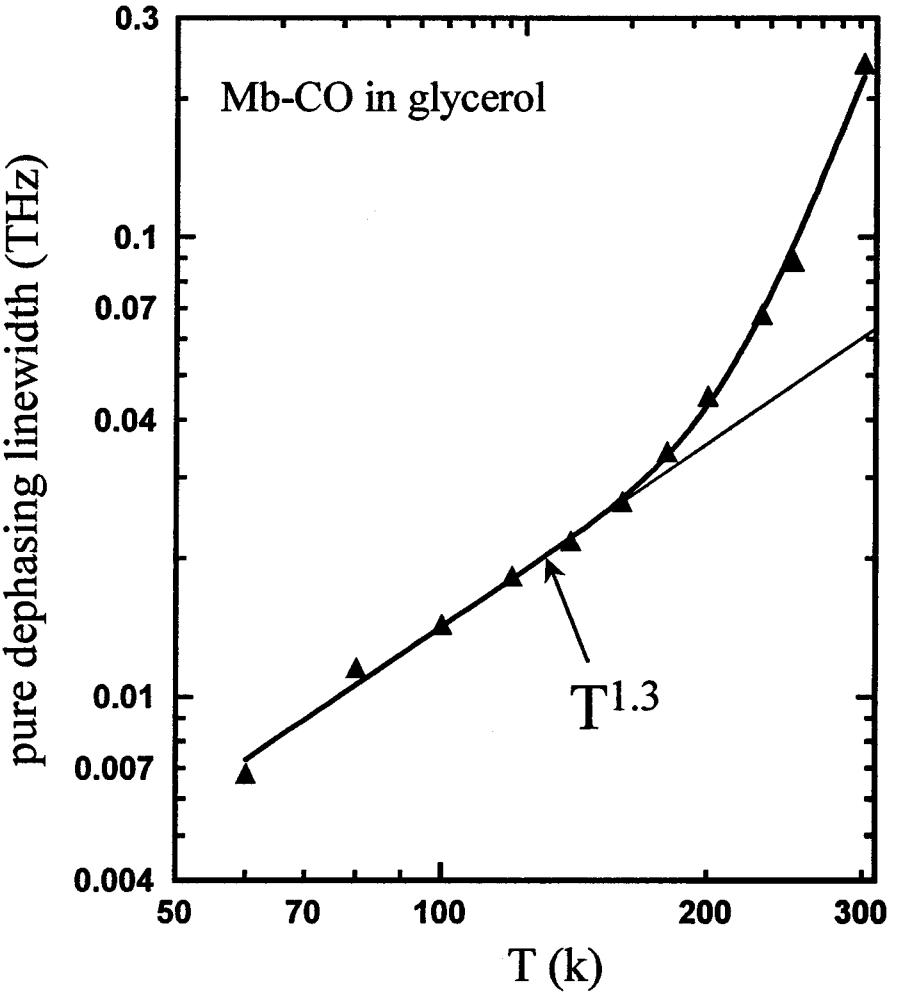

Figure 4 Vibrational echo pure-dephasing line width ($1/\pi T_E^*$) data vs temperature for Mb-CO in glycerol-water. At low temperatures, the temperature dependence is $T^{1.3}$. At higher temperatures, the change in the data with temperature becomes steeper.

the electric field (68–70), whereas the pure dephasing is caused by time-dependent electric fields that arise from the protein's structural dynamics. In either case, the Stark effect is the primary mechanism causing frequency shifts in the CO vibration (47).

To test the fluctuating electric field induced pure dephasing model, experiments were conducted on mutants of Mb-CO (5, 7). Figure 5 displays the temperature-dependent pure dephasing line widths of a mutant of Mb-CO in which the polar

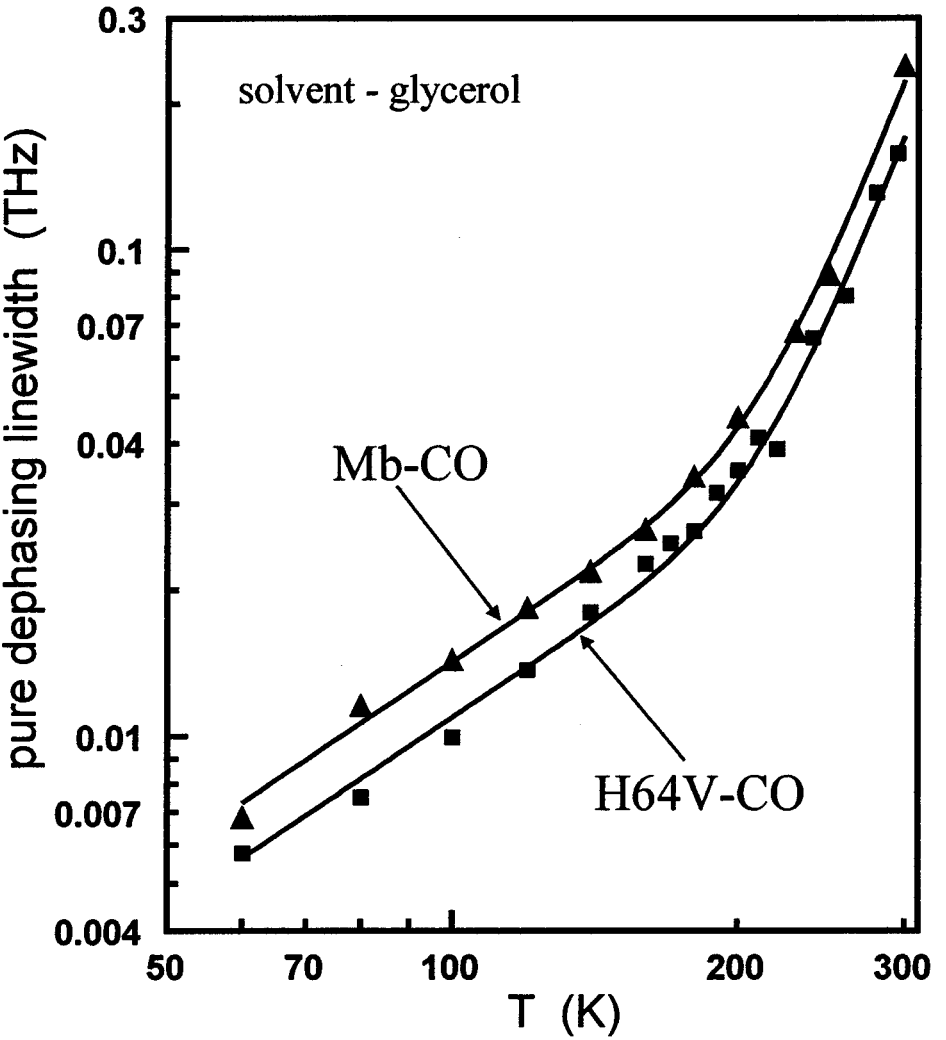

Figure 5 A comparison of the vibrational echo pure-dephasing line width ($1/\pi T_E^*$) data vs temperature for myoglobin Mb-CO and H64V-CO (the mutant with the polar distal histidine replaced with a nonpolar valine) in glycerol-water. The functional forms of the two data sets are identical, but the pure-dephasing line width is ∼20% narrower in H64V-CO at all temperatures. These data support the model stating that pure dephasing is caused by global protein-structural fluctuations that produce a fluctuating electric field at the CO bound at the active site of Mb.

distal histidine is replaced with nonpolar valine (H64V-CO). Also shown in the Figure are the Mb-CO data displayed in Figure 4. The dephasing rate for H64V-CO is slower than for Mb-CO over the entire temperature range. Comparing the data points at each temperature reveals that the H64V-CO rates are ~20% slower than the Mb-CO rates with no systematic variation in the form of the temperature dependence. A solid line was drawn through the H64V-CO data. The line is the same line that runs through the Mb-CO data. The line was translated down with no change in shape. Translation downward on the log plot is the same as multiplying the function that passes through the Mb-CO data by a constant. It can be seen that, within experimental error, the functional forms of the two data sets are identical.

In the H64V-CO experiments, everything about the protein pocket and the experimental procedures is the same as in the previous Mb experiments except for the substitution of the distal histidine with a valine. This amino acid change causes an ~20% reduction in the pure-dephasing rate. Thus, a change in the protein amino acid sequence produces a change in the coupling of the protein fluctuations to the CO ligand bound at the active site. These results strongly support the model that CO pure dephasing is caused by coupling to the protein fluctuations, because a change in the protein with no change in the solvent produces a substantial change in the rate of pure dephasing.

In the fluctuating-electric-field dephasing mechanism, protein motions result in motions of the amino acids. The dynamics of these amino acids, particularly the polar ones, produce fluctuating electric fields at the CO bound to the active site. The fluctuating fields generate time-dependent variations in the CO vibrational frequency via the Stark effect. The fluctuating vibrational frequencies cause the vibrational pure dephasing measured by the vibrational echo.

X-ray crystallographic data of the H64V mutant show that the equilibrium structure of the protein is not significantly different from that of Mb (22). Therefore, it is unlikely that there is a significant change in the global dynamics of the protein. Thus, the functional form of the temperature dependence of the H64V-CO vibrational pure dephasing is unchanged from that of Mb-CO, because it reflects the spectrum of protein fluctuations that are coupled to the CO. However, the strength of the coupling of the protein fluctuations to the CO is reduced because one of the closest sources of the fluctuating electric field has been removed.

As a further test of the electric field model, another mutant, H93G (*N*-methyl-imidazole) [H93G(N-MeIm)]-CO (71, 72) was studied (7). The heme at the active site of Mb has only one covalent linkage to the protein, the iron-H93 bond. H93 is contained in the F α-helix of the globin. In the mutant, the proximal H93 is replaced by glycine, leaving a cavity on the proximal side of the heme (23). Many exogenous ligands (L) to the heme iron, such as imidazoles and pyridines, can be substituted into this cavity, producing a series of proteins—H93G(L)s (71). Although these proteins retain a covalent linkage between the heme iron and the proximal ligand, the covalent connection to the protein backbone is severed. When *N*-methyl-imidazole is used as the exogenous proximal ligand, the hydrogen bond between the proton on the imidazole imino-nitrogen and the hydroxyl group on serine 92 is also absent (72). As with native Mb, the open heme coordination site

on the distal side binds biologically important diatomic molecules such as O_2, CO, and NO. The H93G(N-MeIm) protein has been shown to have a structure very similar to that of native Mb (7, 72). The CO transition frequency and room temperature vibrational CO lifetime of the mutant are almost identical to the native value (72–74).

H93G(N-MeIm)-CO has the only covalent bond between the active site and the protein removed. However, *N*-methylimodazole is essentially the side group as histidine. Therefore, the electrostatic environment is unchanged although the mechanical linkage to the protein is broken, removing the ability of local protein-conformational fluctuations to move the proximal histidine. Such motions could push and pull the Fe in and out of the plane of the heme ring system, changing the CO vibrational frequency and, therefore, causing pure dephasing.

Figure 6 displays temperature dependent, pure dephasing line widths for H93G(N-MeIm)-CO and Mb-CO. Within experimental error, eliminating the covalent bond to the Fe but leaving the electrostatic nature of the protein unchanged does not influence the magnitude or the temperature dependence of the pure dephasing. These vibrational echo measurements give further support to the fluctuating global electric field mechanism. When the polar histidine is replaced by nonpolar valine, H64V-CO, the pure dephasing is reduced (see Figure 5) because one contributor to the fluctuating electric field is gone. The H93G(N-MeIm)-CO experiments show that pure dephasing does not arise from local motions of the Fe-CO caused by movement of H93, but rather that fluctuating electric fields are the dominate cause of pure dephasing in Mb-CO.

Temperature Dependence and the Protein-Glass Transition

Figure 7 shows the pure-dephasing contribution to the line width, $1/\pi T_E^*$, vs temperature on a log plot for Mb-CO in trehalose (10). Trehalose is a glassy solid at all of the experimental temperatures. On a log plot, a power law is a straight line. As can be seen in Figure 7, between 11 and ~200 K, the functional form of the data is a power law,

$$\frac{1}{\pi T_E^*} = aT^{1.3}, \qquad 8.$$

where the prefactor $a = 3.5 \times 10^7 \pm 0.1 \times 10^7$ Hz/(degree K)$^{1.3}$. The error bar on the power law exponent is ± 0.1. This power law is identical to the one in Figure 4. However, the trehalose data are for a much broader range of temperatures and leave little doubt as to the functional form of the data. The same power law was observed in ethylene glycol-water (see below).

In Figure 7, there is a change in the functional form of the data at ~200 K. The points above ~200 K can be fit with

$$\frac{1}{\pi T_E^*} = 3.3 \times 10^{12} \mathrm{e}^{\frac{-650}{k_B T}} \text{ Hz}, \qquad 9.$$

where k_B is Boltzmann's constant, $k_B T$ has units of cm^{-1}, and the error bars on the prefactor and activation energy are $\pm 0.2 \times 10^{12}$ Hz and ± 25 cm^{-1}, respectively.

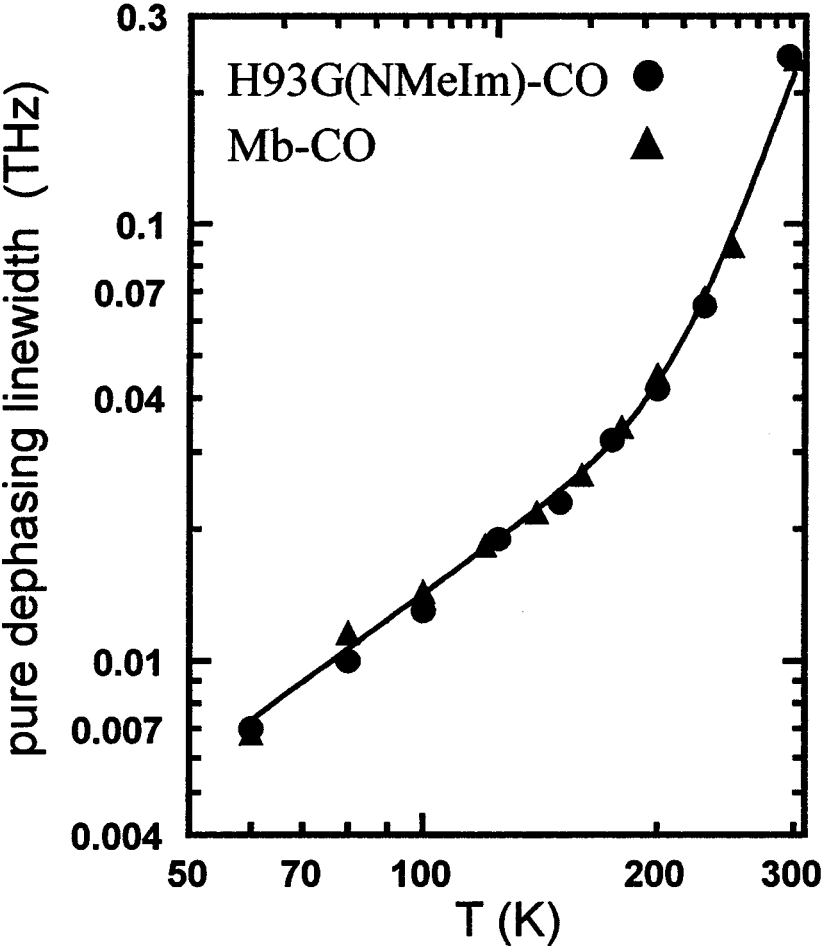

Figure 6 A comparison of the vibrational echo pure-dephasing line width ($1/\pi T_E^*$) data vs temperature for myoglobin Mb-CO and H93G (*N*-methylimidazole)-CO (the proximal histidine is replaced by glycine, and *N*-methylimidazole is the exogenous ligand) in glycerol-water. Within experimental error, the two data sets are identical. Breaking the only covalent bond between the heme and the protein does not change the pure dephasing when the electrostatic environment is unchanged because of the substitution of the histidine side chain with the equivalent *N*-methylimidazole.

It is clear that there is a change in the functional form of the temperature dependence at ~200 K. However, it is important to emphasize that the form of Equation 9 is not unique, given the small number of points. A very good fit is obtained if the data are fit to a power law plus a VTF-type equation (63–65). A VTF equation describes many processes, such as viscosity in super-cooled liquids as they approach the

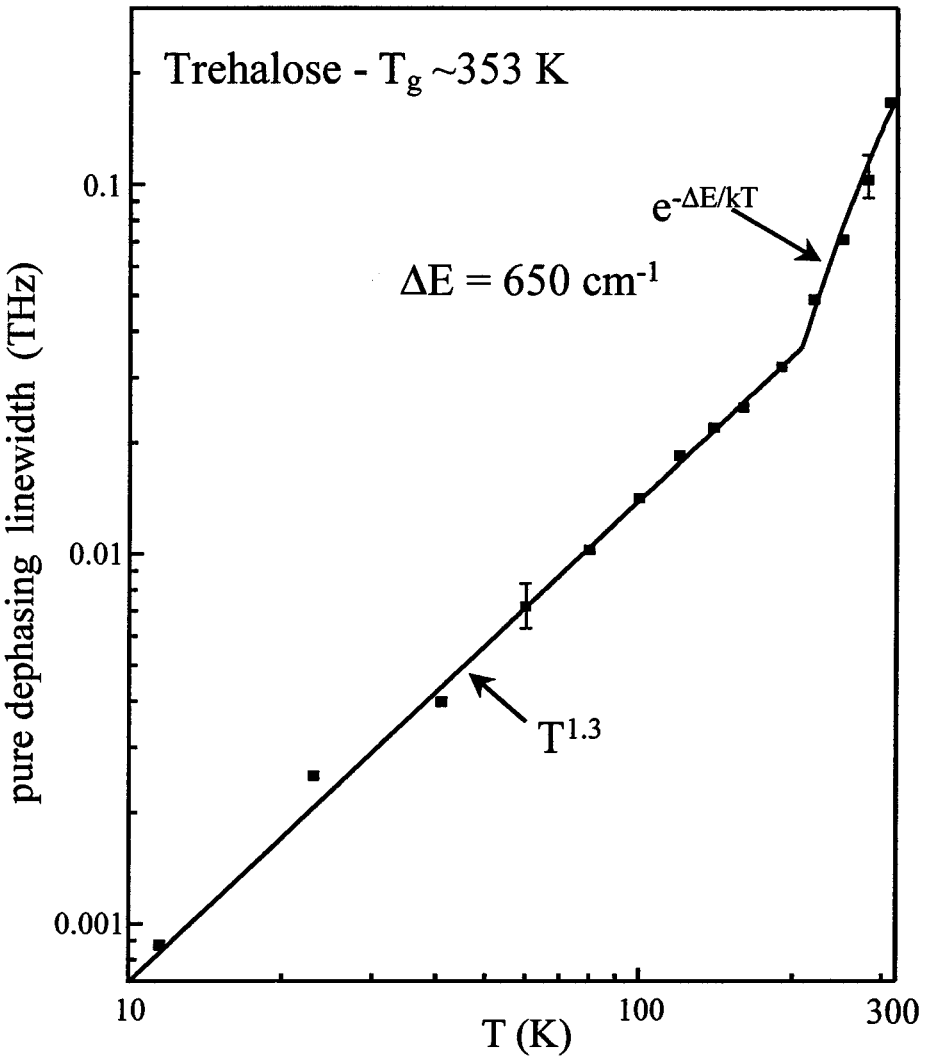

Figure 7 Temperature-dependent pure-dephasing line width ($1/\pi T_E^*$) of Mb-CO in trehalose. Trehalose is a glass at all of the experimental temperatures shown. The data are fit with a power law $T^{1.3}$ below ~200 K and with an exponentially activated process ($\Delta E = 650\ cm^{-1}$) at >200 K. The $T^{1.3}$ temperature dependence is indicative of glasslike behavior, and the break in the temperature dependence may indicate the "protein-glass transition" at ~200 K.

glass transition temperature. The VTF equation for the dynamic line width is

$$\frac{1}{\pi T_E^*} = b e^{\frac{-E}{k_B(T-T_0)}}. \qquad 10.$$

For a true glass-forming liquid, T_0 is the "ideal" glass transition temperature. It typically has a value a few tens of degrees below the laboratory T_g (63–65). A fit to the data with the combination of Equation 8 and Equation 10 yields a T_0 of ∼180 K and an E corresponding to a temperature of ∼230 K. These parameters can vary somewhat about the given values because of the wide range of fits that can be achieved when fitting four points with three parameters. However, the power law is always identical, independent of the form used to fit the points above ∼200 K. If the exponential fit and the VTF fit are extended to higher temperatures, they do not become distinguishable below 500 K. Therefore, experiments at temperatures below the Mb denaturation temperature cannot distinguish these two forms. Regardless of the form that is used to fit the data, it is clear that there is a sudden change in the nature of the temperature dependence of the pure dephasing at ∼200 K, and below ∼200 K, the temperature dependence is $T^{1.3}$.

It has been observed in a wide variety of low-temperature glasses, far below T_g, that the temperature dependence of optical pure dephasing of electronic transitions, measured by photon echo and hole-burning experiments, is a power law and that the typical power law is $T^{1.3}$ (18, 75–78). Heat capacities of low-temperature glass also display power law temperature dependence, again with the value of the exponent being somewhat greater than 1 (53, 79).

Power law temperature dependences of heat capacities and optical dephasing, as well as other observable properties have been explained in terms of the tunneling TLS model of glasses (52, 80). Generally, the TLS model is invoked only below a few K. A power law temperature dependence of the vibrational pure-dephasing line width was observed for a solute in an organic glass up to ∼20 K (9). TLSs in glasses arise from slight differences in local structures. The complex structural energy landscape is modeled as double wells having a broad distribution of energy differences between the two sides of the double well. The dynamics in glasses at low temperatures are caused by phonon-assisted tunneling among local structures modeled as transitions between the two sides of the double wells.

In the Mb-CO vibrational dephasing, the $T^{1.3}$ temperature dependence is observed at much higher temperatures than in true glasses. One possible explanation of the power law temperature dependence is thermally assisted tunneling among slightly different protein configurations. Small internal protein structural changes might be described in terms of protein TLSs (5, 10, 62). The protein TLSs are akin to the TLSs of very low-temperature glasses except that the protein energy landscape would have to be such that tunneling is the dominant process, even at temperatures of ≤200 K. If this is the case, the same statistical mechanics used to describe the low-temperature (∼1 K) optical dephasing of electronic transitions of chromophores in low-temperature glasses (19, 81) can be used to describe the protein TLS-induced vibrational dephasing of Mb-CO at much higher temperatures

(∼100 K). Alternatively, the power law temperature dependence could arise from activation over barriers rather than tunneling, if there is the appropriate energy landscape to provide the necessary broad distribution of activation energies (82, 83). In either case, the $T^{1.3}$ temperature-dependent pure dephasing can occur because of motion on a broad protein energy landscape in a manner analogous to dynamics in true glasses. Although an entirely different mechanism cannot be ruled out, the similarity of the vibrational echo data for Mb-CO to dephasing and other measurements on low-temperature glasses is suggestive of a type of glasslike state of the protein.

Switching from a power law to an activated process or the power law to the VTF function is appropriate if there is a transition in the fundamental nature of the dynamics. There has been considerable discussion in the literature concerning a "protein-glass transition." A glass transition for a bulk material is recognized to be dynamical in nature (64). Below T_g, the system can no longer interconvert on a reasonable time scale among the full range of structural configurations accessed in the liquid. Previous temperature-dependent experiments on Mb-CO have revealed a type of dynamical transition in the protein at ∼200 K that has been referred to as a protein-glass transition (84–86). This is not a glass transition in the normal sense because a transition from a liquid to a glass as temperature is decreased is a phenomenon associated with a bulk material, whereas a protein is a single molecule. However, its complexity is so great that it undergoes continual structural evolution among a vast number of configurations. Below the protein T_g (T_g^P), sampling of protein configurations is greatly slowed. Thus, like a true liquid-glass, a protein may undergo a type of dynamical transition.

The Mb dynamics near ∼200 K, which suggest a protein-glass transition, have been the subject of a considerable number of investigations. For example, inelastic neutron scattering of hydrated Mb at $<$180 K measures only vibrational motion, and at $>$180 K there is a dynamical transition, which is interpreted as the onset of torsional jumps between states (87, 88). Molecular dynamics simulations of the torsional transitions of the dihedral angles of Mb in water show that the anharmonic mean square displacements change at 200 K, which is indicative of a glasslike transition (89). In addition, IR (90–92) and visible (93) transition frequencies, dielectric relaxation (90), specific heat of water in Mb crystals (90), and Mössbauer spectra of ^{57}Fe-Mb (94) all show breaks near 200 K. Some experiments have suggested that this is a "slaved" glass transition; that is, the protein undergoes a transition induced by the true glass transition of the solvent (84–86).

The vibrational echo data presented in Figure 7 may be the strongest evidence for a protein-glass transition at ∼200 K. The solvent is a glass. Therefore, the break in the functional form of the dynamics cannot be ascribed to a change in the nature of the solvent dynamics (see below). The $T^{1.3}$ temperature dependence observed at $<$200 K is the typical temperature dependence observed for photon echo-dephasing measurements, heat capacities, and other experiments in true glasses at low temperatures. If the power law pure vibrational-dephasing temperature dependence below ∼200 K is caused by motion on a glasslike energy

landscape, then data above ~200 K could result from activation above the top of the landscape (64).

Solvent Viscosity and Protein Dynamics

In the experiments with Mb-CO in trehalose, the solvent is a glass at all temperatures studied (10–310 K). Therefore, the dephasing arises from the protein dynamics with a rigid, essentially infinite viscosity solvent. Figure 8 displays data taken in a 50:50 (vol/vol) mixture of ethylene glycol-water (EgOH:H_2O) along with the trehalose data displayed in Figure 7 (10, 47). The EgOH:H_2O sample has a glass transition at ~140 K and a rapidly decreasing viscosity as temperature increases. The dephasing rates in the two solvents are identical ($T^{1.3}$) below ~150 K, at which temperature both solvents have extremely high or infinite viscosity. In contrast, the dynamics are dramatically different above ~150 K, where

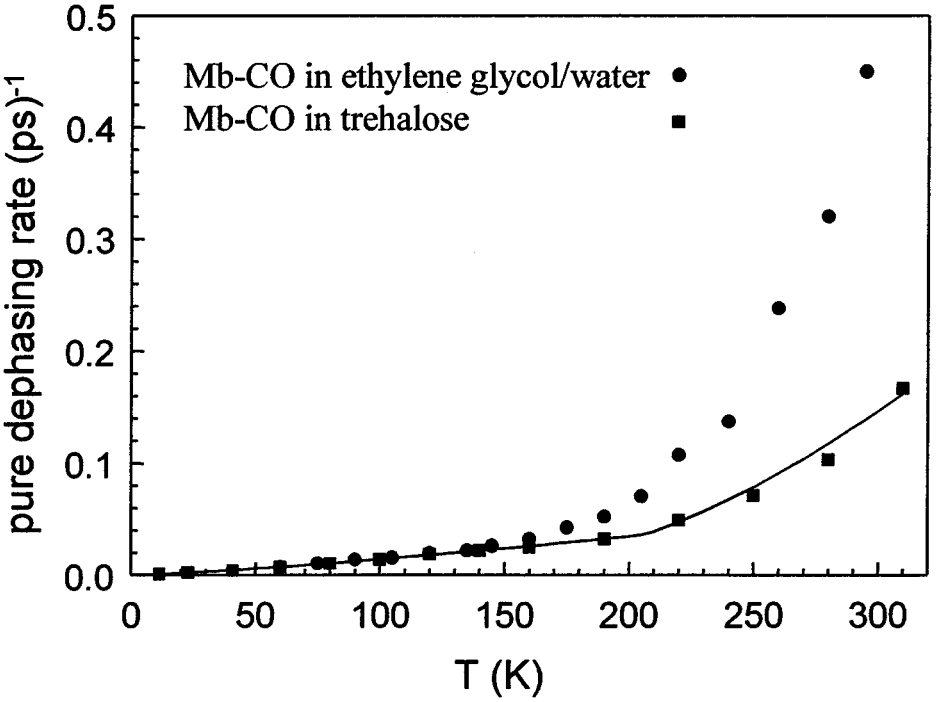

Figure 8 Temperature-dependent pure-dephasing rates ($1/T_E^*$) of Mb-CO in trehalose (*boxes*) and 50:50 ethylene glycol-water [EgOH:H_2O (*circles*)]. The line through the trehalose data is the same as that shown in Figure 7. Trehalose is a glass at all of the experimental temperatures. The EgOH:H_2O with protein solution goes through its glass transition at ~140 K. The data in the two solvents have the identical $T^{1.3}$ temperature dependence at low temperatures, at which both solvents are glasses. Once EgOH:H_2O becomes a liquid, the Mb-CO pure-dephasing rate in this solvent increased rapidly with temperature, compared with the rate measured in trehalose.

the viscosities of the solvents differ substantially. With increasing temperature, the pure-dephasing rate of Mb-CO in the fluid EgOH:H_2O increases much more rapidly than it does in the solid trehalose. The additional dephasing in EgOH:H_2O is consistent with a solvent viscosity effect. However, the viscosity of EgOH:H_2O changes many orders of magnitude between 150 and 295 K, whereas pure dephasing changes only somewhat more than 1 order of magnitude. Given the large change in viscosity and the comparatively small change in the rate of pure dephasing, the relationship between the pure dephasing and solvent viscosity is not immediately apparent.

As discussed below, a comparison of the solvent-dependent and temperature-dependent data shows that the change in the pure dephasing rate with temperature is caused by a combination of viscosity dependence and pure temperature dependence. The dephasing in glassy trehalose (infinite viscosity) is due only to pure temperature-dependent processes. When this contribution is removed from data in fluid solvents, the remaining "reduced" dephasing rate is dependent on only the viscosity of the solvent, whether the solvent viscosity is varied by changing the temperature of a single solvent or by changing the solvent composition at a fixed temperature.

A viscoelastic continuum model is presented to analyze the data (47). The key idea in this model is that the internal dynamics of the protein are strongly constrained by the ability of the protein's surface to move (10, 47). When the protein is embedded in a disordered glass, a variety of surface topologies occur, but each protein molecule is fixed (or nearly fixed) with a single surface topology. Internal fluctuations are restricted to those protein motions that involve little motion at the surface. The vibrational echo decay time of the CO, which is sensitive to the magnitude and rate of the internal structural fluctuations of an individual protein molecule, is slow. When the protein is in a liquid, its surface can move more freely, allowing protein molecules to change their surface topologies. However, just above the glass transition temperature, the solvent is very viscous, and the surface motion is very slow. Internal dynamics connected with surface motion are also slow, and their effect on the echo decay rate remains small. Other dephasing processes that occur in the glass, namely, the vibrational lifetime and the temperature-induced dephasing, overwhelm the contribution of the structural fluctuations enhanced by surface motions, even though the solvent is a liquid. As the solvent viscosity is decreased further (and the temperature is raised), more rapid surface fluctuations permit faster internal protein structural fluctuations. This viscosity-dependent contribution to the echo decay becomes observable and is increasingly important as the viscosity is decreased.

In the model, the protein is taken to be a compressible breathing sphere with surface motions that are constrained by the viscoelastic properties of the solvent. Both the magnitude and correlation time of the thermal fluctuations of the protein's size are calculated. Taking the motions of the surface to be linearly coupled to the CO frequency, the echo decay time is calculated as a function of the solvent viscosity and temperature. A detailed analysis of the properties of the echo experiment in the presence of slow modulation of the transition frequency (54), that is, spectral

diffusion, which is briefly discussed above, is essential to applying the viscoelastic model.

Figure 9 displays isothermal pure-dephasing data as a function of the solvent viscosity (47). The viscosities are varied by changing the solvent. The compositions of the mixtures are given earlier in this review. From Figure 9, it is clear that the Mb-CO pure dephasing is sensitive to the solvent viscosity. These data and the data taken in trehalose support the idea that there is both a temperature-dependent contribution to the dephasing, which does not depend on changing viscosity, and a viscosity dependence that does not depend on changing temperature.

It is possible to quantify the influence of changing viscosity on pure dephasing. At room temperature, the trehalose sample displays significant pure dephasing although the viscosity is essentially infinite. Thus, the pure-dephasing rate in trehalose represents the infinite-viscosity point. The pure dephasing in this sample is due only to temperature-induced structural fluctuations of the protein that do not require participation of solvent motion to any significant extent. To obtain the viscosity dependence, the room temperature infinite-viscosity, pure-dephasing rate, that is, the rate in trehalose, is subtracted from the pure-dephasing rates measured

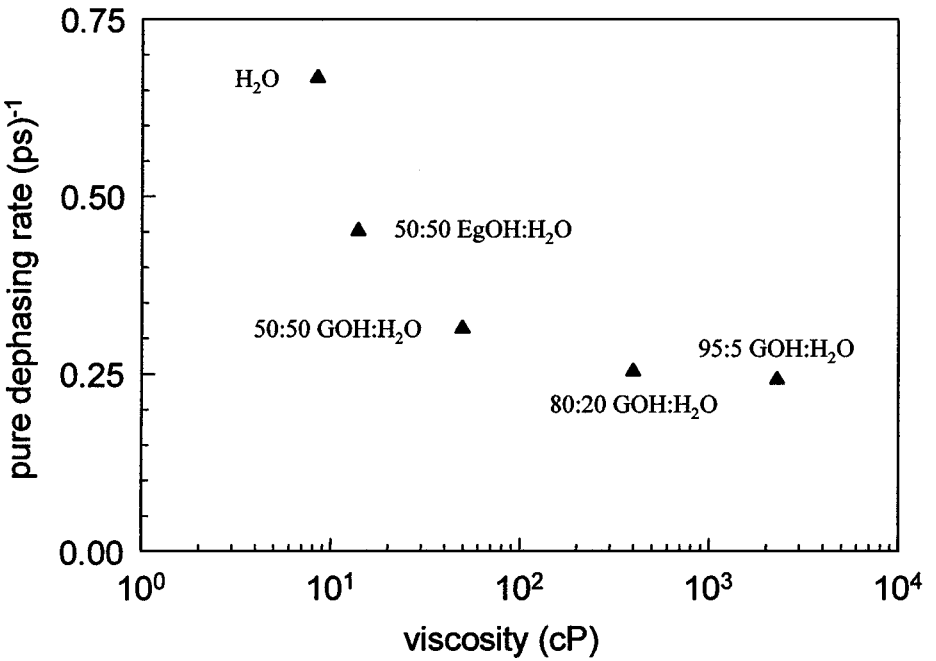

Figure 9 Isothermal (295 K) viscosity-dependent Mb-CO pure-dephasing rates ($1/T_E^*$) in solvents of various compositions (see text). The data demonstrate that the Mb-CO pure dephasing is significantly dependent on viscosity at constant temperature. EgOH, ethylene glycol; GOH, glycerol.

at finite viscosities,

$$\frac{1}{T_E^r(\eta)} = \frac{1}{T_E(\eta, T)} - \frac{1}{T_E(\eta = \infty, T)}, \qquad 11.$$

where T_E^r is the reduced pure dephasing time.

The model in Equation 11 assumes that the temperature-dependent contribution to pure dephasing at infinite viscosity and the viscosity-dependent contribution are additive. The additivity feature of the model can be tested experimentally. Figure 10 is a plot of the reduced isothermal-viscosity-dependent data from Figure 9 (47). The room temperature, infinite-viscosity, pure-dephasing rate was subtracted using Equation 11. Also shown in Figure 10 are data obtained as a function of temperature in 50:50 (vol/vol) EgOH:H_2O (Figure 8). For each EgOH:H_2O

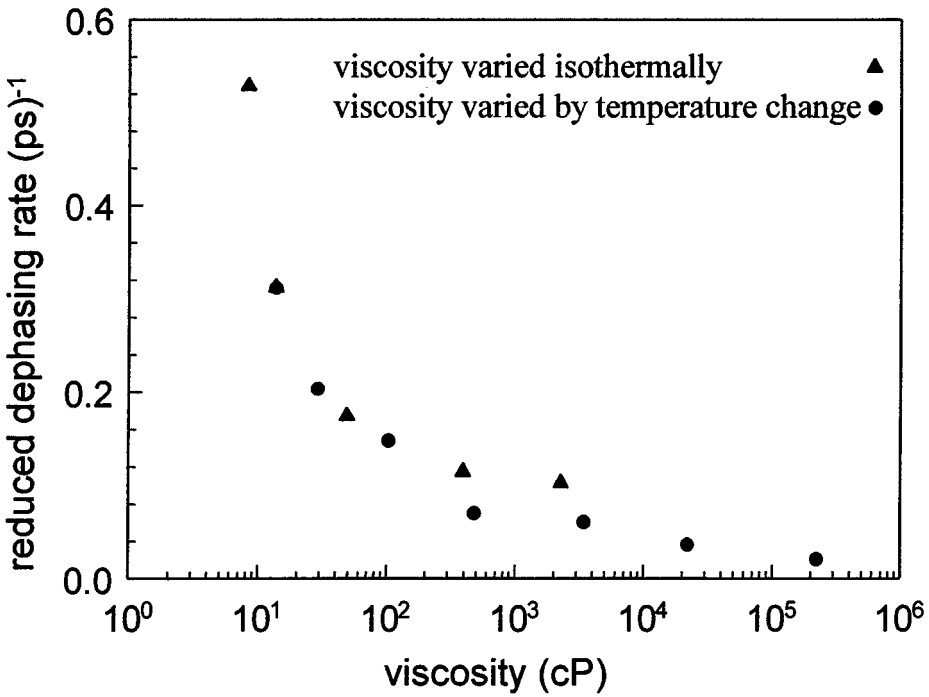

Figure 10 Pure-dephasing rates at a given viscosity minus the 295 K rate at infinite viscosity (see Equation 11). *Triangles*, isothermal (295 K) viscosity-dependent Mb-CO reduced pure-dephasing rates; *circles*, temperature-dependent Mb-CO in 50:50 ethylene glycol-water (EgOH:H_2O) pure-dephasing rates minus the corresponding infinite-viscosity (trehalose data) pure-dephasing rates at each temperature plotted against the viscosity of the EgOH:H_2O protein solution. The *circles* are the viscosity-induced part of the pure dephasing rate at various temperatures. (Note that the point at ~10 cP is an *overlapping circle and triangle*.). The fact that the circles and the triangles are intermixed demonstrates that the viscosity component and the pure-temperature component of the pure-dephasing rates are additive within experimental error.

point, the pure-dephasing rate in trehalose was subtracted. For the points between room temperature and 210 K, the viscosity is known (47), and the differences between the EgOH:H_2O data and the trehalose data are plotted at the appropriate viscosity. Notice that, within experimental error, the isothermal-viscosity points and the viscosity points obtained at various temperatures are intermingled. The trend is the same. Therefore, the infinite-viscosity, pure-dephasing rate and the viscosity-dependent, pure-dephasing rate are additive within experimental error.

The viscosity dependence of the experimental data displays two qualitative features. First, the reduced dephasing rate is almost entirely determined by the solvent viscosity. The detailed chemical properties of the solvent do not make much difference as shown by the isothermal data taken in a variety of solvents (Figure 9). The apparent difference in the temperature dependence between EgOH:H_2O and trehalose (Figure 8) is almost entirely caused by the temperature dependence of the viscosity (Figure 10). It is not obvious that the CO pure dephasing should have a strong sensitivity to the solvent viscosity. The CO is located internally in Mb, precluding a direct interaction between the CO and the bulk solvent. The dephasing is not sensitive to the particular solvent when the solvents are all glasses. The frequency of the Mb-CO stretch is insensitive to the solvent, demonstrating that there is no direct interaction of the solvent with the CO.

The second qualitative result is that the viscosity dependence of the dephasing rate is relatively weak. The data summarized in Figure 10 cover changes of viscosity of >5 orders of magnitude, but the reduced dephasing rate changed by ~ 1.5 orders of magnitude.

These facts can be explained using the following model (47). As discussed above, the change in the frequency, ω, of the CO is directly proportional to the electric field, E, at its site owing to a vibrational Stark shift (47, 68). Fluctuations in the instantaneous configuration of the protein cause fluctuations in this electric field, δE. Taking ω° as the frequency at the time-averaged protein configuration, the time-dependent CO frequency is calculated as

$$\omega(t) = \omega^\circ + \frac{\delta\mu_{01}\delta E(t)}{\hbar}. \qquad 11.$$

The value of the change in dipole moment from the ground to first excited vibrational level, $\delta_{01} = 0.14$ Debye $= 2.4\,\mathrm{cm}^{-1}/(\mathrm{MV/cm})$, has been measured recently (68). When the protein is in a solid, glassy solvent, the surface topology of the protein is essentially fixed. The solvent resists any shearing motions, so the surface of the protein can change only by elastic distortions of the glassy solvent. Because the compressibility of a glass is very low, surface motions of the protein are severely limited. If the internal motions of the protein are strongly coupled to the motion of the surface, the internal protein dynamics are also tightly constrained. The protein can still undergo internal structural fluctuations, but only those fluctuations are permitted that do not move the protein's surface very far. These motions, as sensed by CO bound at the active site of Mb, are reflected in the temperature-dependent, pure-dephasing measured in trehalose. The only feature of the solvent that is

important is that it keeps the protein surface fixed. Thus, in EgOH:H_2O below its T_g, the behavior of Mb-CO is identical to its behavior in trehalose. The pure dephasing of Mb-CO in glycerol-water is also identical at temperatures below that solvent's glass transition (10; see Figure 4).

As the temperature is increased above T_g, a new contribution to the Mb-CO echo decay measurements comes into play. When the solvent is a fluid, the range of motion of the protein's surface and, as a result, the range of its internal motions are much greater. The additional amplitude of the protein motion increases the magnitude of dynamic fluctuations in the electric field at the CO bound in the interior of the protein and thus in the magnitude of dynamic fluctuations in the CO vibrational frequency. However, the viscosity of the solvent determines the rate of this increased motion. Just above T_g, the liquid is extremely viscous, and the increased protein motions are very slow. The effect on the CO echo decay is correspondingly weak. The increased dephasing caused by motions allowed by the solvent is undetectable over the other contributions to the dephasing rate produced by the solvent-independent processeses. That is, just above T_g, the solvent-induced dephasing is still in the quasistatic limit and is eliminated by the echo experiment. In EgOH:H_2O, this is the situation from ~136 to 150 K. The dephasing rate remains almost identical to that in the true glass, trehalose (Figure 8).

As the temperature is increased further, the viscosity of the solvent drops rapidly. At some point, the protein-structural fluctuations dependent on moving its surface become fast enough to have a measurable contribution to the echo decay. The system enters the spectral-diffusion regimen. Further increases in temperature reduce the solvent viscosity and increase the internal protein fluctuation rate by many orders of magnitude. The echo decay rate also increases. However, because of the weak power law connecting the fluctuation time, τ_m, and the echo decay time in the spectral-diffusion region (Equation 6), the echo decay rate increases only weakly with decreasing viscosity, a little over 1 order of magnitude. This region covers ~150–295 K in EgOH:H_2O (Figure 8).

The model gives a good qualitative account of the dephasing rate vs temperature in EgOH:H_2O and in trehalose (47). Moreover, it explains how the CO vibration can be sensitive to the solvent viscosity without any direct coupling between the solvent and the CO. The disparity in the magnitude of change in the viscosity and the echo decay rate is also accounted for.

A recently developed viscoelastic-continuum theory of solvent dynamics (95–97) can be used to make the model quantitative (47). The protein is modeled as a sphere of radius r_p embedded in a viscoelastic and continuous solvent (47). The solvent's viscoelastic behavior is characterized by a decaying shear modulus $G(t)$. For sufficiently short periods, the solvent behaves as a solid with a short-time (infinite-frequency) shear modulus G_∞. At times comparable to or longer than the decay time of $G(t)$, the solvent can flow, allowing additional fluctuation of the protein's surface. This decay time is directly related to the solvent viscosity. The protein is also treated as a continuous material with a bulk modulus K_p. Viscous relaxation or "flow" of the protein in response to its distortion is irrelevant and not

included. With these assumptions, the protein will almost instantaneously transmit changes in its surface to its interior.

Figure 10 shows that the temperature-induced dephasing and the viscosity-induced dephasing are separable within experimental error. In the model, it is assumed that the corresponding protein motions with a frozen surface and the additional motion allowed by moving the surface can be treated as independent processes. The two types of motions need not involve different protein coordinates. Both processes may involve the same internal motions of the protein. The freeing of the surface only increases the amplitude of the motion along the same coordinates that cause the viscosity-independent dephasing. It is also possible that the protein has conformational changes that relax much more slowly than the solvent. Any change in the CO frequency due to these conformations will be in the quasistatic limit and will not contribute to the vibrational echo decay. The viscoelastic model treats only the viscosity-dependent dephasing reflected in the reduced dephasing time $T_E^r(\eta)$.

The protein's fluctuations are fully characterized by its change in radius $\delta r_{\rm p}$ (47). Changes in radius are linked to changes in the electric field at the CO, because of displacements of charged groups within the protein. The details of the coupling are not treated. Rather, a phenomenological proportionality constant b is used, and

$$\delta E(t) = b\delta r_p(t). \qquad 12.$$

The viscosity-dependent protein dynamics in the model (47) are now equivalent to the structural dynamics in other viscoelastic models (95–97). The magnitude of the thermal fluctuations in the protein radius is given by

$$\left\langle \delta r_p^2 \right\rangle = \frac{kT}{12\pi K_p r_p}, \qquad 13.$$

where k is the Boltzmann constant. Combining Equations 11, 12, and 13, the magnitude of the CO frequency modulation is

$$\Delta_m = \left\langle (\omega(0) - \omega^\circ)^2 \right\rangle^{1/2} = \frac{b\delta\mu}{\hbar\sqrt{4\pi}} \left(\frac{kT}{3K_p r_p} \right)^{1/2} = \Delta_0 \left(\frac{T}{T_0} \right)^{1/2}, \qquad 14.$$

where $\omega(0)$ is the frequency at $t = 0$. The most important feature of Equation 14 is the temperature dependence of $\Delta_{\rm m}$. The temperature-independent constants are collected into Δ_0, the modulation amplitude at the reference temperature T_0. Here, $T_0 = 295$ K.

The relaxation time of the thermal fluctuations is proportional to the solvent viscosity, with the proportionality constant determined by the solvent and protein moduli, as follows:

$$\tau_m = \alpha \frac{\eta}{G_\infty}, \qquad 15.$$

and

$$\alpha = 1 + \frac{4G_\infty}{3K_p}. \qquad 16.$$

As an estimate, $K_p \approx K_\infty$, and the Cauchy relation for simple solids can be used (98), such that $G_\infty = (3/5)K_\infty$, giving $\alpha \approx 9/5$. Using the value for water (99) gives an estimate $G_\infty \approx 10 \times 10^{10}$ dyne/cm^2. Over the experimental range of viscosities of $\sim 10^1$–10^6 cP, modulation times in the approximate range 2 ps–200 ns are expected.

The echo response can be calculated using Equations 14–16 under a wide variety of conditions. Given the long modulation times predicted, it is reasonable to take the system to be in the spectral-diffusion regime $\tau_m \Delta_m \gg 1$. Using Equations 4, 5, 14, and 15, gives

$$T_E \sqrt{\frac{T}{T_0}} = C \left(\eta(T) \sqrt{\frac{T}{T_0}} \right)^{\frac{\beta}{\beta+2}}, \qquad 17.$$

and

$$C = B_\beta \Gamma\left(\frac{1}{\beta+2}\right)\left(\frac{\alpha^\beta}{G_\infty^\beta \Delta_0^2}\right)^{\frac{1}{\beta+2}}. \qquad 18.$$

The dominant source of temperature dependence in Equation 17 is the viscosity, which has a steep VFT (63–65) dependence on temperature. The constants in Equation 18 can be approximated as temperature independent. The moduli are actually temperature dependent, but this dependence is relatively weak (100). In Equation 17, other than the viscosity, the only temperature dependence is the explicit square root of the temperature, which is weak.

Thus, the viscoelastic theory explains why the solvent viscosity is the dominant factor in determining the dephasing rate (47). Furthermore, for reasonable values of β, that is, near unity, the dephasing rate varies with the viscosity raised to a small fractional power. Again, the theory is in accord with the relatively weak dependence on viscosity observed in the experiments.

The viscoelastic theory was tested quantitatively as shown in Figures 11 and 12 (47). In Figure 11, both the isothermal and temperature-dependent data are included. Equation 17 predicts a linear relationship on this log plot, with a positive slope. If the system were in the fast modulation limit, then the slope would be negative, and if there were a shift between the fast modulation limit (motional narrowing) and the slow modulation limit (spectral diffusion) as the viscosity changes, then there would be a change in the sign of the slope and a minimum in the curve (54). The slope remains positive over the entire viscosity range, so the assumption that the system is in the spectral diffusion regime is valid.

The line in Figure 11 has the slope predicted by Equation 17 for $\beta = 1$, which in turn corresponds to a cube-root dependence of the dephasing rate on the viscosity. The line shows quite good agreement with the data. The points at the highest viscosities fall off the line, but these are the points with the greatest uncertainty in the viscosities. $\beta = 1$ corresponds to an exponential decay of the CO frequency-frequency correlation function and, consequently, of the solvent shear modulus

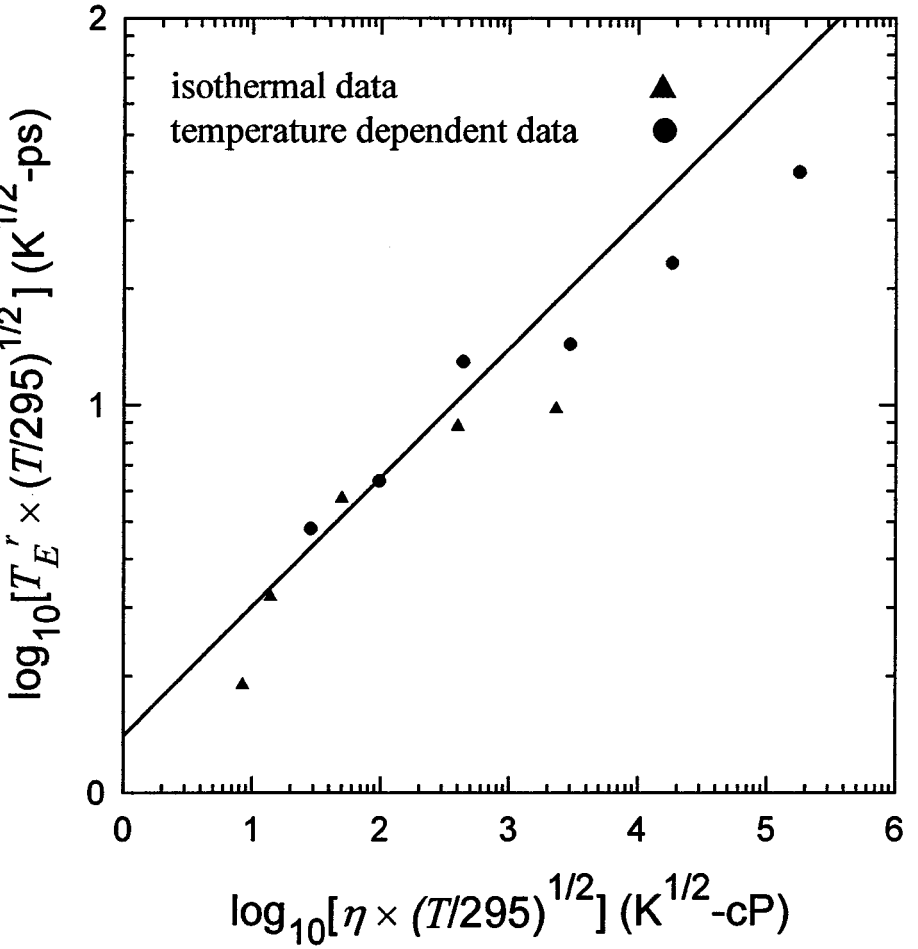

Figure 11 The reduced-echo pure-dephasing time from both the isothermal (*triangles*) and temperature-dependent (*circles*) measurements are plotted against viscosity in accord with Equation 17. The line corresponds to the cube root dependence on viscosity predicted for an exponentially relaxing shear modulus ($\beta = 1$). The line also corresponds to the fit shown in Figure 12.

(54). It is common for shear modulus relaxation functions to become nonexponential at high viscosity, which would lead to a smaller value of β. This effect could also contribute to the deviations seen at the highest viscosities.

The solid line in Figure 12 displays the fit of the reduced dephasing rate from Figure 11, combined with the viscosity-independent dephasing data taken in trehalose (Equations 8 and 9) to recreate the full temperature-/viscosity-dependent dephasing rate in EgOH:H_2O (47). The theory does a remarkable job of reproducing the data qualitatively and essentially quantitatively. It misses the lowest

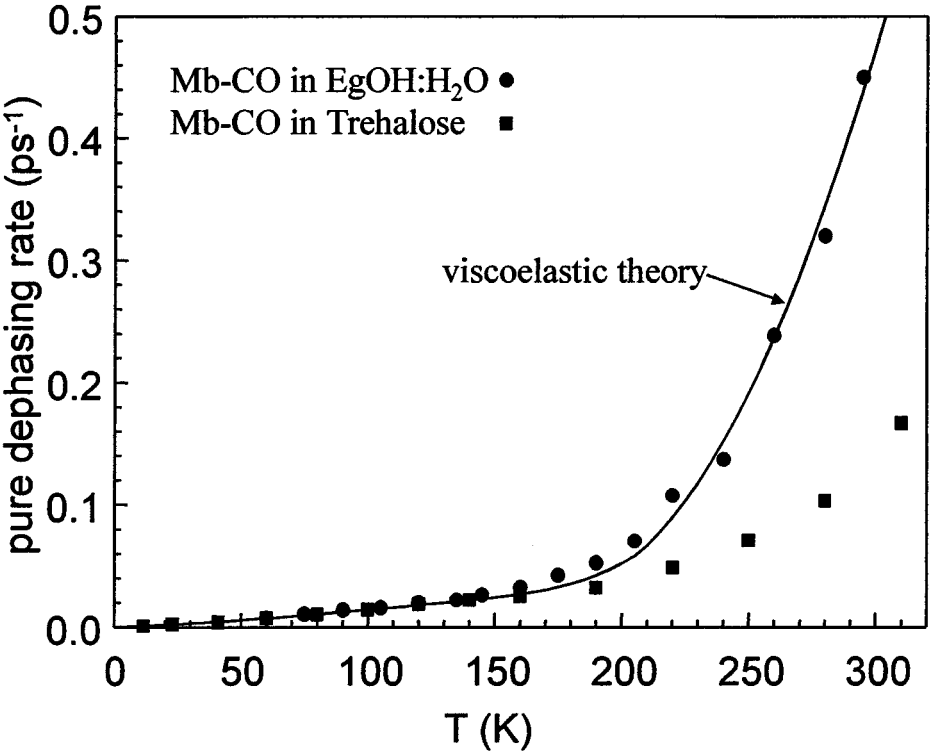

Figure 12 Temperature-dependent Mb-CO pure-dephasing rates ($1/T_E^*$) in trehalose (*squares*) and in 50:50 ethylene glycol-water (EgOH:H_2O; *circles*). The line through the EgOH:H_2O data is the fit to the viscoelastic theory (Equation 17) added to the temperature dependence in trehalose. The viscoelastic theory attributes the difference between the trehalose and EgOH:H_2O rates to fluctuations of the protein surface that are governed by the solvent viscosity. The theory does a remarkable job of reproducing the data. These results confirm the importance of the role of protein surface fluctuations in the internal protein structural fluctuations responsible for CO pure dephasing.

temperature points somewhat, possibly either for the reasons discussed above or because of an inherent limitation of the theory. The calculated curves in Figure 11 and Figure 12 are different methods of comparing theory and experiment.

The viscosity-dependent dephasing in EgOH:H_2O is active at temperatures below the putative protein-glass transition (see Figures 7 and 8). As discussed above, the Mb-CO pure-dephasing data in trehalose have a break at $\sim$200 K that may be caused by the protein-glass transition (10). Although the viscosity-independent dephasing in trehalose shows a break, the additional viscosity-dependent dephasing that occurs in EgOH:H_2O does not show an observable break at the protein-glass transition. This observation is compatible with the viscoelastic theory. Within the

theory, the response of the solvent is governed by its shear relaxation, but the protein responds only through its compressibility (J Jiang and MA Berg, personal communication). For typical liquids, the compressibility changes only ~20% at the glass transition (102, 103). If the change in protein compressibility at the protein-glass transition were similarly small, no observable break in the internal dynamics connected with surface motion would be expected. This conclusion is supported by computer simulations, which have shown that there is not a dramatic change in the dynamical behavior of Mb across the protein-glass transition (20, 21). Thus, the viscoelastic theory predicts that the viscosity-dependent dephasing mechanism should remain active below the protein-glass transition, as is observed experimentally. In general, the solvent viscosity can influence a protein's dynamics even below its glass transition. Another possible reason that viscosity-dependent dephasing in EgOH:H_2O is observed at <200 K is a shift in the protein-glass transition to a lower temperature in the liquid solvent (10). This idea is supported by the fact that, in a system such as a thin polymer film, which has a large surface-to-volume ratio in which the surface is free to move, the T_g shifts below that of the bulk material (104).

The fits in Figures 11 and 12 are very good considering that there is only one adjustable parameter, C (Equations 17 and 18). The fit gives $C = 1.4$ ps/cP$^{1/3}$ (47). Using Equations 14 and 18, the value of b corresponding to the fit can be obtained. With $\delta\mu_{01} = 0.14$ Debye, an average protein radius of 3.5 nm, and the previous estimate $\alpha \approx 9/5$, it is found that $b \approx 8.3 \times 10^3$ dyne/Debye.

The fit value of C can be used to place a bound on Δ_0 (47). Detailed analysis (47) gives $1.1\ \text{ps}^{-1} \leq \Delta_0 \leq 1.2\ \text{ps}^{-1} = \Delta_I$ where Δ_I is the inhomogeneous line width. This is an important result. The process responsible for the viscosity-dependent spectral diffusion accounts for almost all of the IR line width. Therefore, the viscosity-dependent protein fluctuations responsible for the vibrational echo decay on a relatively fast time scale span a very broad range of time scales. The results suggest that there are no other distinctly different slow processes responsible for the inhomogeneous line width. Increasingly slower spectral diffusion of the same nature as that measured on fast time scales by the vibrational echo experiments accounts for essentially the entire absorption line.

Taking $\Delta_0 \approx \Delta_I$ along with Equation 18, the previous estimate of $\alpha \approx 9/5$ and the measured value of C gives a value for the solvent shear modulus: $G_\infty = 15 \times 10^{10}$ dyne/cm^2. For comparison, the value for pure water is shown as $G_\infty = 11 \times 10^{10}$ dyne/cm^2 (99). Given the errors in the experimental fit and in the estimated parameters, this inferred value of G_∞ is very reasonable. (Implicit in the analysis is an assumption that the value of this modulus is independent of solvent composition and temperature. Errors in this approximation can lead to some of the scatter around the fit.). The fit value of G_∞ then leads to an estimate of the protein modulation time in the various solvents through Equation 15, $\tau_m \approx (0.12\ \text{ps/cP})\eta$. Thus, a quantitative estimate of the viscosity-dependent modulation time is obtained from the vibrational echo experiments.

A number of imprecisely known factors contribute to a moderate level of uncertainty in all of the above estimates. However, they should be accurate enough to

establish with some certainty the parameters involved in solvent-induced protein dynamics. The fact that all of these numbers are internally self-consistent as well as compatible with physical expectations strongly supports the model and the values of parameters obtained from the data analysis.

The viscosity-dependent vibrational echo results reveal a fundamentally important property of proteins. The internal structural fluctuations of proteins are intimately related to the surface fluctuations and the viscoelastic properties of the medium in which the protein is embedded. The data in the glassy solvent trehalose shows that a protein's structure fluctuates even when the surface topology of the protein is fixed. However, in a liquid solvent like ethylene glycol-water, structural fluctuations of the protein are greatly enhanced because internal evolution of the protein's structure requiring changes in the protein's surface topology is permitted.

The viscoelastic model fits the data using physically reasonable parameters. The viscosity-dependent echo decay time is proportional to $\eta^{1/3}$, where η is the solvent viscosity. This behavior is characteristic of dephasing caused by spectral diffusion (relatively slowly evolving CO frequency) with an exponential frequency-frequency correlation function (54). The entire experimental region lies within the spectral diffusion and quasistatic regions; that is, motional narrowing of the CO vibrational line is not observed. The success of the model in describing both the isothermal (solvent-dependent) viscosity data and the temperature-dependent viscosity data supports the underlying concept that the solvent plays an important role in protein structural dynamics through its influence on protein surface motions, which in turn have a substantial affect on the internal structural dynamics of the protein (47).

Vibrational Echo Experiments on Hemoglobin-CO

Human Hb A is a tetrameric protein composed of two α and two β subunits. The intrinsic differences in the subunits' ligand affinities and the interactions between them are necessary for the proper functioning of Hb (105). When isolated, the subunits exhibit different behavior from that of the $\alpha_2\beta_2$ tetramer (106). The CO stretch of carbonmonoxy Hb (Hb-CO) at room temperature displays a dominant peak, C_{III} at $\sim$1951 with a full width at half maximum of $\sim$8 cm^{-1}. From difference absorption spectroscopy, it is known that the subunits have slightly different absorbencies. The α and β subunits' maximum absorbencies are at 1950.5 cm^{-1} and 1951.6 cm^{-1}, respectively (106). This difference indicates that the CO ligands' environments are not identical in the two subunits. The Mb protein has three distinct CO-stretching modes, which have relative amplitudes that are sensitive to changes in pH, temperature, and amino acid sequence (107). In Mb-CO, the dominant line, A_1, is $\sim$75% of the integrated band area, whereas in Hb, the C_{III} line is $>$96% (106, 108).

The secondary and tertiary structures of Mb are similar to those of the α and β subunits of intact Hb (109). The similarities in structures are noteworthy because the primary sequences of the three chains are the same at only 24 of 141 positions

(31). Most of these differences are subtle changes of size or polarity, such as a leucine in Hb_α and Mb at F1, where a phenylalanine is found in Hb_β. Some differences are more dramatic, such as F7 in which a serine occurs in Mb but an alanine occurs in Hb_α and Hb_β (31). These changes in amino acid polarity do not significantly change the secondary or tertiary structure of Hb. However, changes in the polarity will change the electrostatic nature of the protein.

Vibrational echo studies were performed on Hb-CO using an IR OPA pumped by a regenerative amplified Ti:Sapphire system rather than the FEL. The advent of Ti:Sapphire-based commercial equipment capable of generating tunable mid-IR pulses that are useful for performing detailed vibrational echo studies of proteins and other systems is expanding the application of vibrational echo methods to a wide variety of problems.

For the experiments on Hb-CO, the bandwidth of the IR pulses was limited to avoid pumping to higher vibrational levels of the CO mode (2, 110) and to have the bandwidth of the IR pulses approximately the same as the line width. The bandwidth is limited by placing a slit in the stretcher. The output of the regenerative amplifier has wings generated by the sharp cutoff of the bandwidth caused by the slit. However, the bandwidth is narrowed slightly, and the wings are eliminated by the use of a grating and four consecutive nonlinear processes in the OPA used to generate the IR. The IR pulses are 900 fs in duration and have nearly Gaussian shape as determined by IR autocorrelation. The IR bandwidth was $\sim$18 cm^{-1}. At 5 μm, the OPA typically produces 6–7 μJ/pulse at 1 kHz.

The experimental vibrational echo setup used with the OPA system is very similar to that used with the FEL (see Figure 2). However, single-pulse selection is not necessary since the Ti:Sapphire-OPA system has a repetition rate of 1 KHz. One of the beams was chopped at 500 Hz, and a lock-in amplifier was used in the detection. Pulse energies up to $\sim$4 μJ/pulse were available at the sample. Power studies were performed at high and low temperatures to ensure that there were no intensity or heating artifacts.

The sample was prepared from human Hb in a manner similar to that used for the Mb-CO samples (37). The concentration was $\sim$18 mmol in a 50:50 (vol/vol) ethylene glycol (EgOH)-phosphate buffer (pH 7) mixture. Thermal stability of proteins is not greatly affected by relatively high concentrations of EgOH (111–113), and concentrations $\leq$22 mol% are not thought to cause structural perturbations.

Fourier transform IR spectra were recorded as a function of temperature across the temperature range of the echo experiments. The room temperature peak was centered at 1951.8 cm^{-1} and had a width of 8.0 cm^{-1} and an absorbance of 0.5 on a 1.2 background. The peak center and width changed slightly and monotonically as the temperature was lowered. By 50 K, the peak center had shifted to 1949.3 cm^{-1}, and the width had grown to 8.1 cm^{-1}. The OPA wavelength was tuned to the absorption center at each temperature, so the α and β CO modes were both driven (37).

Figure 13 displays a vibrational echo decay measurement taken with the Ti: Sapphire/OPA system. These data are for Hb-CO in EgOH-H_2O, at 40 K. Also shown is an exponential fit to the decay data. The decay time is 11.0 ps, yielding

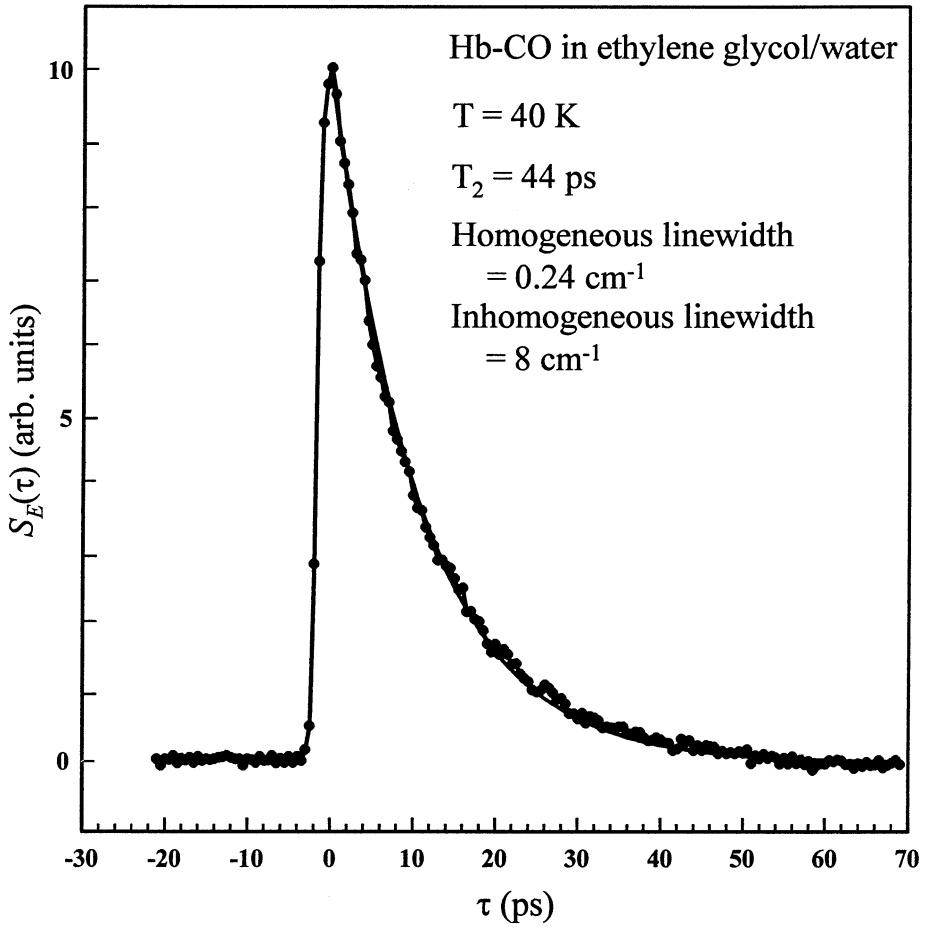

Figure 13 An example of vibrational echo data taken on Hb-CO in ethylene glycol-water and a single exponential fit to the data. The data were taken at 40 K. The decay time was 11.0 ps, giving a T_2 of 44.0 ps; the corresponding homogeneous line width was 0.24 cm^{-1}. The inhomogeneous line width was 8 cm^{-1}. The absorption line was inhomogeneously broadened at all temperatures studied.

a T_2 of 44 ps. These echo data were taken on a sample in which the protein had a very strong background absorption compared with that of the CO peak under study. Nonetheless, it is possible to obtain high-quality vibrational echo data. The data took approximately 10 min to acquire.

Figure 14 displays the pure-dephasing rates for Hb-CO as a function of temperature and a comparison to the pure dephasing rates of Mb-CO, both in EgOH-H_2O. As can be seen from the figure, Hb-CO- and Mb-CO-dephasing data have the same functional form and differed only in the magnitudes of their pure-dephasing rates. The Mb-CO data are the same as shown in Figure 8 (10). The line through the

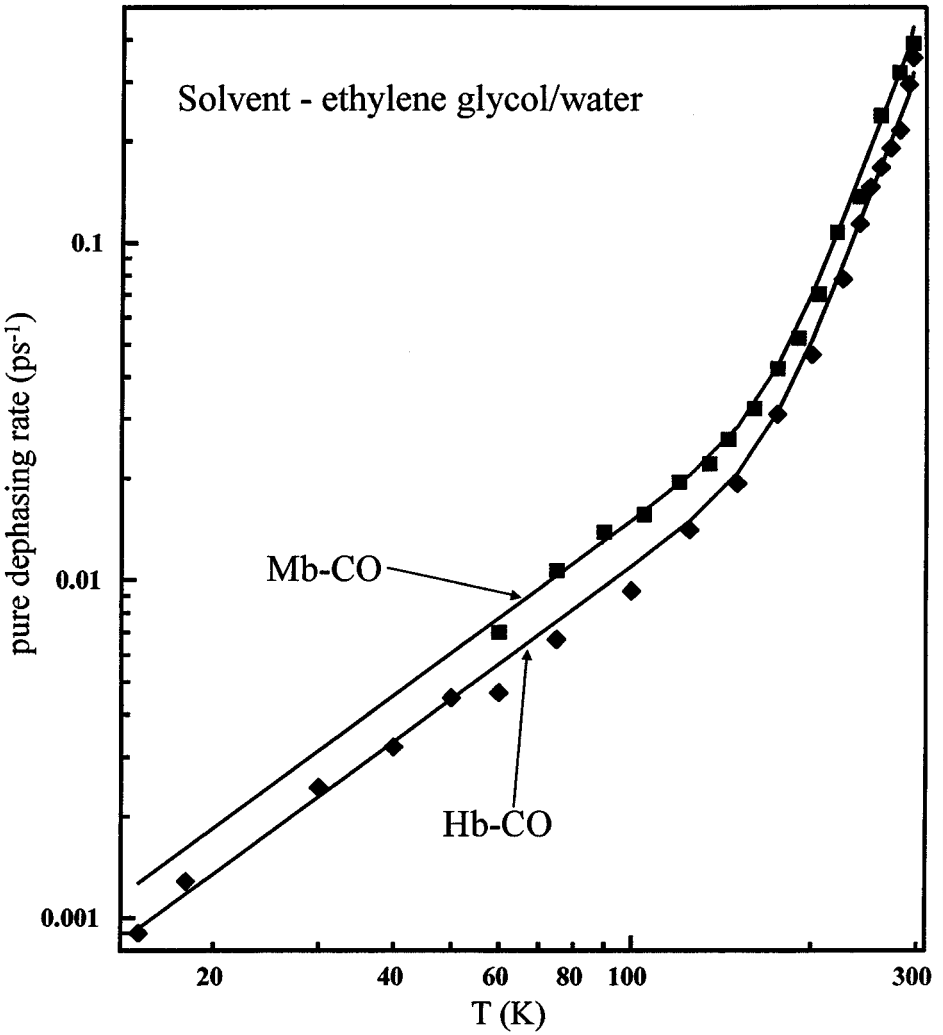

Figure 14 Pure-dephasing rates of Hb-CO and Mb-CO, both in glycerol-water, on a log plot. The data from Mb-CO were the same as in Figure 8. The line through the Hb-CO data is the line though the Mb-CO data multiplied by the constant 0.73. The functional forms of the temperature dependences were identical.

Mb-CO data is not from the viscoelastic theory (Figure 12). It is an empirical fit of the form given in Equations 8 and 9, that is, a $T^{1.3}$ power law at low temperature and an exponentially activated function at high temperature (10). This form is used to put a line through the Mb-CO data to make possible a direct comparison to the Hb-CO data. The line through the Hb-CO data is not a fit; rather, it is the Mb-CO fit multiplied by a constant factor 0.73. These results show that the

functional form of the temperature-dependent pure-dephasing dynamics of Hb-CO is identical to Mb-CO, but the pure dephasing in Hb-CO is 27% slower across the entire temperature range.

As proposed above, the source of the pure dephasing in Mb-CO involves motions of the polar groups in the protein that generate fluctuating electric fields at the CO (47). This model is supported by mutant studies and analysis of data using the viscoelastic theory. A possible explanation for the reduction in the rate of pure dephasing in Hb-CO compared with Mb-CO (Figure 14) is that the magnitudes of the fluctuating electric field at the CO in Hb-CO are less than in Mb-CO. The fluctuating electric field in Hb-CO may be reduced either because of the differences in the locations of polar groups or because the protein dynamics on the time scales observed by the vibrational echo experiment are reduced in Hb-CO compared with Mb-CO. Hb is approximately fourfold greater in volume than Mb. The change in surface-to-volume ratio could influence the viscoelastic response of the protein. The fact that, within experimental error, the functional form of the pure-dephasing temperature dependence in Hb-CO is identical to that in Mb-CO demonstrates that the fast global dynamics of the two proteins, as sensed by the CO ligand bound at the active sites of the proteins, are very similar. This suggests that the distributions of barriers controlling structural fluctuations have the same nature in the two proteins.

CONCLUDING REMARKS

The application of ultrafast IR vibrational echo experiments to the study of proteins is a new approach for the investigation of protein dynamics. To date, Mb-CO has been studied extensively, and initial experiments have been conducted on Hb-CO. For both proteins, pure vibrational dephasing of the CO ligand bound at the active sites of the protein provides information on the global structural fluctuations of the protein. Temperature-dependent, vibrational echo, pure-dephasing measurements have been made on Mb-CO in a variety of solvents and on two mutants of Mb-CO. In addition, the isothermal (300 K) viscosity dependence of Mb-CO pure dephasing has been measured.

The temperature-dependent, vibrational echo results show that the pure dephasing of the Mb mutant, H64V-CO, is $\sim$21% slower than that of native Mb-CO with no change in the functional form of the temperature dependence. The temperature dependence of the pure dephasing of the mutant H93G(N-MeIm)-CO is identical to that of the native Mb-CO. The general mechanism proposed to explain the coupling of conformational fluctuations of the protein to the vibrational-transition energy of CO bound at the active site is supported by these results. The model states that global protein motions produce a fluctuating electric field that is responsible for the CO pure dephasing via a direct Stark effect (68) on the CO vibrational frequency (47). Replacing the polar distal histidine with the nonpolar valine (H64V-CO) removes one source of the fluctuating electric field, thus reducing the coupling between the protein fluctuations and the measured pure dephasing. The picture

that emerges is that the CO bound at the active site acts as an antenna for the fluctuating electric fields produced by the protein dynamics, providing an avenue for study of protein-structural fluctuations through vibrational echo measurements of pure dephasing.

At low temperature, the pure vibrational dephasing of Mb-CO in several solvents and Hb-CO have the same $T^{1.3}$ power law temperature dependence. This power law temperature dependence is the signature of glass dynamics in low-temperature glasses and suggests that the protein has passed through a "protein-glass transition." In the solvent trehalose, which is a glass at all of the experimental temperatures, the pure dephasing of Mb-CO displays a transition from $T^{1.3}$ to a steeper temperature dependence above ~200 K. The break in the temperature dependence is consistent with a protein-glass transition at ~200 K.

Mb-CO in liquid solvents displays much steeper pure-dephasing temperature dependence than it does in the glassy-solvent trehalose. The increased temperature dependence is a combination of pure temperature dependence and viscosity dependence. As the temperature is increased, the solvent viscosity decreases, leading to an additional contribution to pure dephasing. The existence of viscosity dependence is confirmed by an isothermal viscosity-dependent pure-dephasing study. The influence of viscosity on protein dynamics arises from the coupling of the protein internal structure to its surface topology. In a glassy solvent, the surface topology is essentially fixed. Only those protein motions that can occur without changing the surface topology are permitted. As the solvent viscosity decreases, the protein's surface becomes increasingly free to move, enabling protein-structural fluctuations that require changes in the surface topology. The viscosity-dependent behavior of Mb-CO pure dephasing was described quantitatively using a viscoelastic theory of the pure dephasing (47). Nearly quantitative agreement was found between theory and experiment. The theory permits the time scales and nature of viscosity-dependent protein structural fluctuations to be delineated.

The application of ultrafast IR vibrational echoes, related pulse sequences, and multidimensional IR vibrational echo methods to problems of biological interest is just beginning. Most biological and chemical processes occur on the electronic ground state potential surface. They involve structural transformations induced by structural fluctuations. The structural, that is, mechanical, degrees of freedom of molecules are described in terms of the molecular vibrations. Structural dynamics are vibrational dynamics. Vibrational echo techniques, which directly probe vibrational dynamics, will be an increasingly important probe for fundamental biological and chemical processes.

ACKNOWLEDGMENTS

Many people contributed to this work. In particular, I thank Dr. Kirk Rector, currently at Los Alamos National Laboratory, Los Alamos, NM, who was the driving force behind the experiments. I give special thanks to Professor Mark A. Berg, Department of Chemistry and Biochemistry, University of South Carolina,

Columbia, SC, who was primarily responsible for the viscoelastic theory of the protein pure dephasing. All of the Mb-CO experiments were conducted at the Stanford Free Electron Laser Center. I thank Professor H. Alan Schwettman and Professor Todd I. Smith and their students and staff at the Stanford FEL Center for their help and collaboration on many of the experiments. I also thank Professor Dana D. Dlott, Department of Chemistry, University of Illinois, Urbana, IL, who was a major participant in a number of the experimental studies described here. The research described in this review was supported by the National Institutes of Health (grant 1RO1-GM61137) and by the National Science Foundation (grant DMR-0088942).

LITERATURE CITED

1. Zimdars D, Tokmakoff A, Chen S, Greenfield SR, Fayer MD. 1993. *Phys. Rev. Lett.* 70:2718–21
2. Tokmakoff A, Kwok AS, Urdahl RS, Francis RS, Fayer MD. 1995. *Chem. Phys. Lett.* 234:289–95
3. Tokmakoff A, Fayer MD. 1995. *J. Chem. Phys.* 102:2810–36
4. Rella CW, Kwok A, Rector KD, Hill JR, Schwettman HA, Dlott DD, Fayer MD. 1996. *Phys. Rev. Lett.* 77:1648–51
5. Rector KD, Rella CW, Kwok AS, Hill JR, Sligar SG, Chien EYP, Dlott DD, Fayer MD. 1997. *J. Phys. Chem. B* 101:1468–75
6. Rector KD, Kwok AS, Ferrante C, Francis RS, Fayer MD. 1997. *Chem. Phys. Lett.* 276:217–23
7. Rector KD, Engholm JR, Hill JR, Myers DJ, Hu R, Boxer SG, Dlott DD, Fayer MD. 1998. *J. Phys. Chem. B.* 102:331–33
8. Rector KD, Zimdars DA, Fayer MD. 1998. *J. Chem. Phys.* 109:5455–65
9. Rector KD, Fayer MD. 1998. *J. Chem. Phys.* 108:1794–1803
10. Rector KD, Engholm JR, Rella CW, Hill JR, Dlott DD, Fayer MD. 1999. *J. Phys. Chem. A* 103:2381–87
11. Rector KD, Fayer MD, Engholm JR, Crosson E, Smith TI, Schwettmann HA. 1999. *Chem. Phys. Lett.* 305:51–56
12. Hahn EL. 1950. *Phys. Rev.* 80:580–87
13. Schmidt-Rohr K, Spiess HW. 1994. *Multidimensional Solid-State NMR*. London: Academic
14. Kurnit NA, Abella ID, Hartmann SR. 1964. *Phys. Rev. Lett.* 13:567–70
15. Abella ID, Kurnit NA, Hartmann SR. 1966. *Phys. Rev. Lett.* 14:391–94
16. Molenkamp LW, Wiersma DA. 1985. *J. Chem. Phys.* 83:1–9
17. Vainer YG, Personov RI, Zilker S, Haarer D. 1996. In *Int. Meet. Hole Burning Relat. Spectrosc. Sci. Appl., 5th*, Brainerd, Minn, ed. GJ Small, 291:51–55. Brainerd, Minn: Gordon & Breach
18. Berg M, Walsh CA, Narasimhan LR, Littau KA, Fayer MD. 1988. *J. Chem. Phys.* 88:1564–87
19. Narasimhan LR, Littau KA, Pack DW, Bai YS, Elschner A, Fayer MD. 1990. *Chem. Rev.* 90:439–57
20. Elber R, Karplus M. 1987. *Science* 235:318–21
21. Vitkup D, Ringe D, Petsko GA, Karplus M. 2000. *Nat. Struct. Biol.* 7:34–38
22. Quillin ML, Arduini RM, Olson JS, Phillips GN Jr. 1993. *J. Mol. Biol.* 234:140–55
23. Barrick D. 1994. *Biochemistry* 33:6546–54
24. Tsuda S. 1996. *Crystallogr. Soc. Jpn.* 38:84–92

25. Clore GM, Gronenborn AM. 1991. *Prog. Nucl. Magn. Reson. Spectrosc.* 23:43–92
26. Braunstein DP, Chu K, Egeberg KD, Frauenfelder H, Mourant JR, Nienhaus GU, Ormos P, Sligar SG, Springer BA, Young RD. 1993. *Biophys. J.* 65:2447–54
27. Jackson TA, Lim M, Anfinrud PA. 1994. *Chem. Phys.* 180:131–40
28. Janes SM, Dalickas GA, Eaton WA, Hochstrasser RM. 1988. *Biophys. J.* 54:545–49
29. Oldfield E, Guo K, Augspurger JD, Dykstra CE. 1991. *J. Am. Chem. Soc.* 113:7537–41
30. Surewicz WK, Mantsch HH. 1996. In *Spectroscopic Methods for Determining Protein Structure in Solution*, ed. HA Havel, pp. 135–62. New York: VCH Publ.
31. Stryer L. 1988. *Biochemistry.* New York: Freeman
32. Beece D, Eisenstein L, Frauenfelder H, Good D, Marden MC, Reinisch L, Reynolds AH, et al. 1980. *Biochemistry* 19:5147–57
33. Gordon RG. 1968. *Adv. Magn. Reson.* 3:1–17
34. Gordon RG. 1965. *J. Chem. Phys.* 43: 1307–12
35. Tokmakoff A, Zimdars D, Urdahl RS, Francis RS, Kwok AS, Fayer MD. 1995. *J. Phys. Chem.* 99:13310–320
36. Oxtoby DW. 1981. *Annu. Rev. Phys. Chem.* 32:77–101
37. Rector KD, Thompson DE, Merchant K, Fayer MD. 2000. *Chem. Phys. Lett.* 316:122–28
38. Loring RF, Mukamel S. 1985. *J. Chem. Phys.* 83:2116–28
39. Bai YS, Fayer MD. 1989. *Phys. Rev. B.* 39:11066–84
40. Farrar TC, Becker DE. 1971. *Pulse and Fourier Transform NMR*. New York: Academic
41. Skinner JL, Andersen HC, Fayer MD. 1981. *J. Chem. Phys.* 75:3195–202
42. Hahn EL. 1953. *Phys. Today* 6:4–7
43. Brewer RG, Hahn EL. 1984. *Sci. Am.* 251:50–57
44. Rector KD, Fayer MD. 1998. *Int. Rev. Phys. Chem.* 17:261–306
45. Leeson DT, Wiersma DA. 1995. *Phys. Rev. Lett.* 74:2138–41
46. Thijssen HPH, Dicker AIM, Völker S. 1982. *Chem. Phys. Lett.* 92:7–12
47. Rector KD, Jiang J, Berg M, Fayer MD. 2001. *J. Phys. Chem.* In press
48. Levenson MD. 1982. *Introduction to Nonlinear Laser Spectroscopy*. San Jose, Calif.: Academic
49. Slichter CP. 1989. *Principles of Magnetic Resonance*. Berlin: Springer-Verlag
50. Anderson PW. 1954. *J. Phys. Soc. Jpn.* 9:316–39
51. Kubo R. 1961. In *Fluctuation, Relaxation and Resonance in Magnetic Systems*, ed. D Ter Haar. London: Oliver & Boyd
52. Anderson PW, Halperin BI, Varma CM. 1972. *Philos. Mag.* 25:1–7
53. Phillips WA. 1981. *Amorphous Solids: Low Temperature Properties, Topics in Current Physics*. Berlin: Springer-Verlag
54. Berg MA, Rector KD, Fayer MD. 2000. *J. Chem. Phys.* 113:3233–42
55. Mukamel S. 1995. *Principles of Nonlinear Optical Spectroscopy*. New York: Oxford Univ. Press
56. Ma J, Fourkas JT, Vanden Bout DA, Berg M. 1997. In *Supercooled Liquids: Advances and Novel Applications*, Vol. 676, ed. JT Fourkas, D Kivelson, U Mohanty, KA Nelson, pp. 199–211. Washington, DC: Am. Chem. Soc.
57. Klauder JR, Anderson PW. 1962. *Phys. Rev.* 125:912–22
58. Hu P, Hartmann SR. 1974. *Phys. Rev. B* 9:1–13
59. Hu P, Walker LR. 1978. *Phys. Rev. B* 18:1300–1305
60. Yan YJ, Mukamel S. 1991. *J. Chem. Phys.* 94:179–90
61. Tokmakoff A, Fayer MD. 1995. *J. Chem. Phys.* 103:2810–36
62. Rella CW, Rector KD, Kwok AS, Hill JR,

Schwettman HA, Dlott DD, Fayer MD. 1996. *J. Phys. Chem.* 100:15620–29
63. Angell CA, Smith DL. 1982. *J. Phys. Chem.* 86:3845–52
64. Angell CA. 1988. *J. Phys. Chem. Solids* 49:863–71
65. Fredrickson GH. 1988. *Annu. Rev. Phys. Chem.* 39:149–80
66. Ansari A, Beredzen J, Braunstein D, Cowen BR, Frauenfelder H, et al. 1987. *Biophys. Chem.* 26:337–55
67. Ivanov D, Sage JT, Keim M, Powell JR, Asher SA, Champion PM. 1994. *J. Am. Chem. Soc.* 116:4139–40
68. Park E, Andrews S, Boxer SG. 1999. *J. Phys. Chem.* 103:9813–17
69. Oldfield E, Guo K, Augspurger JD, Dykstra CE. 1991. *J. Am. Chem. Soc.* 113:7537–41
70. Augspurger JD, Dykstra CE, Oldfield E. 1991. *J. Am. Chem. Soc.* 113:2447–51
71. DePillis GD, Decatur SM, Barrick D, Boxer SG. 1994. *J. Am. Chem. Soc.* 116:6981–51
72. Decatur SM, DePillis GD, Boxer SG. 1996. *Biochemistry* 35:3925–32
73. Hill JR, Tokmakoff A, Peterson KA, Sauter B, Zimdars DA, Dlott DD, Fayer MD. 1994. *J. Phys. Chem.* 98:11213–19
74. Hill JR, Dlott DD, Rella CW, Peterson KA, Decatur SM, Boxer SG, Fayer MD. 1996. *J. Phys. Chem.* 100:12100–107
75. Walsh CA, Berg M, Narasimhan LR, Fayer MD. 1986. *Chem. Phys. Lett.* 130:6–11
76. Walsh CA, Berg M, Narasimhan LR, Fayer MD. 1987. *J. Chem. Phys.* 86:77–87
77. Thijssen HPH, Volker S. 1985. *Chem. Phys. Lett.* 120:496–502
78. Thijssen HPH, van den Berg R, Volker S. 1985. *Chem. Phys. Lett.* 120:503–8
79. Vohringer P, Arnett DC, Yang TS, Scherer NF. 1995. *Chem. Phys. Lett.* 237:387–98
80. Phillips WA. 1972. *J. Low Temp. Phys.* 7:351–58
81. Leeson DT, Wiersma DA, Fritsch K, Friedrich J. 1997. *J. Phys. Chem. B* 101:6331–40
82. Gilroy KS, Phillips WA. 1981. *Philos. Mag. B.* 43:735–46
83. Kohler W, Zollfrank J, Friedrich J. 1989. *Phys. Rev. B* 39:5414–24
84. Iben IET, Basunstein D, Doster W, Frauenfelder H, Hong MK, et al. 1989. *Phys. Rev. Lett.* 62:1916–19
85. Parak F, Frauenfelder H. 1993. *Physica A* 201:332–45
86. Frauenfelder H, Sligar SG, Wolynes PG. 1991. *Science* 254:1598–603
87. Doster W, Cusack S, Petry W. 1989. *Nature* 337:754–56
88. Loncharich RJ, Brooks BR. 1990. *J. Mol. Biol.* 215:439–55
89. Steinbach PJ, Brooks BR. 1993. *Proc. Natl. Acad. Sci. USA* 90:9135–39
90. Doster W, Bachleitner A, Dunau R, Hiebl M, Luscher E. 1986. *Biophys. J.* 50:213–19
91. Hong MK, Draunstein D, Cowen BR, Frauenfelder H, Iben IET, et al. 1990. *Biophys. J.* 58:429–36
92. Mayer E. 1994. *Biophys. J.* 67:862–73
93. Cordone L, Cupane A, Leone M, Vitrano E. 1988. *J. Mol. Biol.* 199:213–18
94. Parak F, Knapp EW, Kucheida D. 1982. *J. Mol. Biol.* 161:177–94
95. Berg MA, Hubble HW. 1998. *Chem. Phys.* 233:257–66
96. Berg M. 1998. *J. Phys. Chem.* 102:17–30
97. Berg MA. 1999. *J. Chem. Phys.* 110:8577–88
98. Zwanzig R, Mountain RD. 1965. *J. Chem. Phys.* 43:4464–69
99. Bertolini D, Tani A. 1995. *Phys. Rev. E* 52:1699–710
100. Piccirelli R, Litovitz TA. 1957. *J. Acoust. Soc. Am.* 29:1009–115
101. Deleted in proof
102. Litovitz TA, Davis DM. 1965. In *Physical Acoustics*, Vol. IIA, ed. WP Mason. New York: Academic

103. Harrison G. 1976. *The Dynamic Properties of Supercooled Liquids*. New York: Academic
104. Forrest JA, Dalnoki-Veress K, Dutcher JR. 1997. *Phys. Rev. E.* 56:5705–16
105. Weber G. 1982. *Nature* 300:603–7
106. Potter WT, Hazzard JH, Kawanishi S, Caughey WS. 1983. *Biochem. Biophys. Res. Commun.* 116:719–25
107. Caughey WS, Shimada H, Choc MC, Tucker MP. 1981. *Proc. Natl. Acad. Sci. USA* 78:2903–7
108. Karavitis M, Fronticelli C, Brinigar WS, Vasquez GB, Militello V, Leone M, Cupane A. 1998. *J. Biol. Chem.* 273:23740–49
109. Antonini E, Brunori M. 1971. *Hemoglobin and Myoglobin in Their Reactions with Ligands*. Amsterdam: Elsevier/North-Holland Biomed.
110. Rector KD, Kwok AS, Ferrante C, Tokmakoff A, Rella CW, Fayer MD. 1997. *J. Chem. Phys.* 106:10027–36
111. Haire RN, Hedlund BE. 1983. *Biochemistry* 22:327–34
112. Back JF, Oakenfull D, Smith MD. 1979. *Biochemistry* 18:5191–96
113. Gerlsma SY, Stuur ER. 1972. *Proc. Natl. Acad. Sci. USA* 74:4135–38